

## Vasculogenic mimicry structures in melanoma support the recruitment of monocytes

Lih Y. Tan<sup>a</sup>, Michaelia P. Cockshell <sup>a</sup>, Eli Moore <sup>a</sup>, Kay K. Myo Min <sup>a</sup>, Michael Ortiz<sup>a</sup>, M. Zahied Johan <sup>a</sup>, Brenton Ebert<sup>a</sup>, Andrew Ruszkiewicz <sup>a</sup>, Michael P. Brown<sup>a,b,c</sup>, Lisa M. Ebert <sup>a,b,c,\*</sup>, and Claudine S. Bonder <sup>a,b,\*</sup>

<sup>a</sup>Centre for Cancer Biology, University of South Australia and SA Pathology, Adelaide, Australia; <sup>b</sup>Adelaide Medical School, University of Adelaide, Adelaide, Australia; <sup>c</sup>Royal Adelaide Hospital, Cancer Clinical Trials Unit, Adelaide, Australia

### ABSTRACT

The progression of cancer is facilitated by infiltrating leukocytes which can either actively kill cancer cells or promote their survival. Our current understanding of leukocyte recruitment into tumors is largely limited to the adhesion molecules and chemokines expressed by conventional blood vessels that are lined by endothelial cells (ECs). However, cancer cells themselves can form their own vascular structures (a process known as vasculogenic mimicry (VM)); but whether they actively participate in the recruitment of leukocytes remains to be elucidated. Herein, we demonstrate that VM-competent human melanoma cell lines express multiple adhesion molecules (e.g. CD44, intercellular adhesion molecule (ICAM)-1 and junction adhesion molecules (JAMs)) and chemokines (e.g. CXCL8 and CXCL12) relevant for leukocyte recruitment. Microfluidic-based adhesion assays revealed that similar to ECs, VM-competent melanoma cells facilitate the rolling and adhesion of leukocytes, particularly monocytes, under conditions of shear flow. Moreover, we identified ICAM-1 to be a key participant in this process. Transwell assays showed that, similar to ECs, VM-competent melanoma cells facilitate monocyte transmigration toward a chemotactic gradient. Gene expression profiling of human melanoma patient samples confirmed the expression of numerous leukocyte capture adhesion molecules and chemokines. Finally, immunostaining of patient tissue microarrays revealed that tumors with high VM content also contained higher numbers of leukocytes (including macrophages). Taken together, this study suggests an underappreciated role of VM vessels in solid tumors via their active participation in leukocyte recruitment and begins to identify key adhesion molecules and chemokines that underpin this process.

### ARTICLE HISTORY

Received 6 August 2021  
Revised 17 December 2021  
Accepted 31 January 2022

### KEYWORDS

Melanoma; adhesion molecules; monocytes; ICAM-1; chemokines; vasculogenic mimicry

### Introduction

Melanoma is the deadliest form of skin cancer and contributes to 70% of skin cancer-related fatalities.<sup>1</sup> The development of targeted therapies (including BRAF and MEK inhibitors) and immunotherapy (e.g. PD-1 and CTLA-4 inhibitors) has resulted in markedly improved survival prospects for metastatic melanoma patients. However, not all patients respond to these therapies and, of patients who do respond, many develop drug resistance, leaving these patients without effective treatments and a dismal prognosis. A better understanding of tumor biology would pave the way for new targets to be identified and new treatment options to be developed.

Melanoma tumors can be immunogenic and a balance may exist between the anti-tumorigenic CD8<sup>+</sup> T cells and NK cells, which may struggle to penetrate the periphery<sup>2,3</sup> and the pro-tumorigenic regulatory T cells<sup>4</sup> and tumor associated macrophages (TAM),<sup>5</sup> which tend to dominate with disease progression. In order to exert their anti-/pro-tumorigenic functions, leukocytes must physically enter into the tumor. Tumor infiltrating leukocytes cross the endothelial cell (EC) barrier of the blood circulatory system using a multistep process that is orchestrated by the interplay of complementary molecules on the leukocytes and endothelium. Briefly, circulating leukocytes

first tether and roll by interacting with the selectins (E-selectin/P-selectin) and/or hyaluronic acid (HA)-bound CD44 on the endothelium (reviewed in)<sup>6,7</sup> Subsequent interactions between integrins on leukocytes and immunoglobulin superfamily adhesion molecules (e.g. intracellular adhesion molecule-1 (ICAM-1) and vascular cell adhesion molecule-1 (VCAM-1)) on the endothelium promote firm adhesion onto the blood vessel wall.<sup>6,7</sup> This firm adhesion requires the activity of chemokines anchored on the endothelium, which induce conformational changes in integrins necessary for adhesion. Finally, leukocytes interact with junctional adhesion molecules (JAMs) to penetrate through the vasculature and into the underlying tumor mass.<sup>6,7</sup>

The restricted expression of adhesion molecules and chemokine receptors on leukocyte subsets allows selective recruitment into various tissues, including tumors. However, cancer cells in a vascularized tumor mass may alter this selectivity by rendering the tumor vascular endothelium 'anergic' through prolonged exposure to such factors as vascular endothelial growth factor (VEGF) and transforming growth factor beta (TGFβ)<sup>8–10</sup> so that lower levels of P-selectin, E-selectin, ICAM-1 and VCAM-1 are expressed than their counterpart vessels in adjacent tissues.<sup>3,11,12</sup> Tumor ECs also produce less

CCL4, CCL5, CXCL9, CXCL10, and CXCL11,<sup>13,14</sup> key ligands required to recruit cytotoxic CD8<sup>+</sup> T lymphocytes.<sup>15,16</sup> Notably, in line with these reduced adhesive systems on tumor ECs, there remains a paucity of data on mechanisms underlying the recruitment of circulating monocytes (and subsequent accumulation of pro-tumorigenic TAMs) into the tumor bed.<sup>7,17,18</sup>

Our current understanding of leukocyte recruitment to solid tumors is limited to the conventional EC-lined tumor vessels. However, alternative vascular structures exist within many solid tumors that are not lined by ECs, but are lined by the cancer cells themselves. Vasculogenic mimicry (VM) is a process whereby cancer cells mimic EC behavior and align along a deposited basement membrane to form lumenised interconnecting vessel-like structures that perfuse blood and fuse to the endothelium.<sup>19–21</sup> VM has been increasingly recognized as a feature of aggressive cancers with increased metastatic potential<sup>22,23</sup> with studies demonstrating that blocking VM *in vivo* can inhibit tumor growth.<sup>24,25</sup> A meta-analysis of >3,600 cancer patients across 11 different diseases documented that VM vessels can be present in up to 45% of human melanoma<sup>26</sup> and is supported by our own observations that VM vessels contribute ~30% of the total tumor vasculature within melanoma (Bonder *et al.*, manuscript in preparation). More importantly, the presence of VM vessels correlates with increased metastasis and poor overall survival of cancer patients.<sup>26,27</sup>

Interestingly, melanoma cells are documented to express adhesion molecules and chemokines, which were thought to be largely restricted to ECs and which may thus facilitate leukocyte recruitment.<sup>19,28–30</sup> Despite tumor beds containing leaky vasculature wherein transcellular holes and intercellular openings facilitate the influx and efflux of proteins and cells,<sup>31</sup> there is an intriguing possibility that VM vessels have the potential to directly regulate leukocyte trafficking. In particular, these molecules may allow melanoma cells lining VM channels to actively recruit specific immune cell populations from the circulation to promote tumor growth.

Based on these observations, we contend that VM-competent melanoma cells may express adhesion molecules and chemokines to actively (and selectively) recruit leukocyte subsets. Building on our previous publication documenting VM-competent human melanoma,<sup>32</sup> here we examine these cell lines for their expression of various adhesion molecules and chemokines typically described to facilitate leukocyte recruitment by ECs and assess their ability to actively participate in leukocyte adhesion and transmigration.

## Materials and methods

### Ethics statement

The use of buffy coats for isolation of bulk mononuclear cells was given ethics approval by the Central Adelaide Local Health Network (CALHN) Human Research Ethics Committee (HREC) (#130308) and the University of South Australia HREC (#202135). Buffy coats were supplied by

the Australian Red Cross Blood Service. Formalin-fixed paraffin embedded (FFPE) tissue microarray (TMA) of 114 patient melanoma tissues were obtained from SA Pathology (Adelaide, South Australia) as approved by the CALHN HREC (#100123). The isolation of human endothelial cells (ECs) from healthy donors was approved by the human ethics committees of the Royal Adelaide Hospital and the University of South Australia HREC (#201187). All work has been performed in compliance with the current NHMRC code for ethical conduct and to the standards set by the Declaration of Helsinki.

### Cells, cell lines, and cell culture

The human melanoma cell line C32 was purchased from CellBank Australia (Westmead, NSW, Australia), all others were gifted from Prof. G McArthur (Peter MacCallum Cancer Centre, Melbourne, Vic, Australia) and cultured as published.<sup>32</sup> A variety of human ECs were used throughout the study, including the trabecular human bone marrow endothelial cell line (TrHBMEC, gifted from B Weksler, Cornell University Medical College, New York, NY, USA<sup>33</sup>), human umbilical vein endothelial cells (HUVEC) from consented healthy umbilical cords<sup>34</sup> and endothelial colony-forming cells (ECFCs) from healthy human peripheral blood<sup>35</sup> and grown in RPMI supplemented with 10% FBS (RF10).

### Matrigel tubulogenesis assays

For the *in vitro* vascular assays,  $1.5 \times 10^4$  ECFCs or  $\sim 2 \times 10^4$  melanoma cells (C32, CHL-1, SK-Mel-28, MeWo and M238) were seeded per well onto 10  $\mu$ l of Growth Factor Reduced/normal Matrigel (Corning, Corning, NY, USA) in angiogenesis  $\mu$ -slides (Ibidi, Munich, Germany) for up to 24 h. Time-lapse videos of the network formation were captured via the live cell imaging microscope CellVoyager CV1000 Yokogawa Spinning disk Confocal Scanner (Olympus Life Science, Tokyo, Japan).

### RNA extraction and sequencing

RNA was isolated from C32, CHL-1, and SK-Mel-28 cells using the mirVana™ miRNA isolation kit (Ambion™, Life Technologies, Carlsbad, CA, USA) as per manufacturer's instructions. Samples were multiplexed and sequenced on the Illumina NextSeq 500 platform (2 runs) using the stranded single end protocol with a read length of 75. Raw reads were adaptor trimmed and filtered for short sequences using cut-adapt v1.3,<sup>36</sup> setting minimum-length option to 18, error-rate 0.2, overlap 5 and a quality score cut-off of 28. The resulting FASTQ files averaging 18.5 M reads per sample were processed via the FastQC program (<http://www.bioinformatics.babraham.ac.uk/projects/fastqc>). The filtered reads were mapped against the human reference genome (Hg19) using the TopHat spliced alignment algorithm<sup>37</sup> (version 2.0.9 with default parameters) returning an average alignment rate of 97%. Counts of reads mapping to each gene were calculated using HTSeq

v0.6.1p1.<sup>38</sup> Differential expression analysis was evaluated from TMM normalized gene counts using R (version 3.2.3) and edgeR (version 3.3)<sup>39</sup> following protocols as described in Chen et al. and Lun et al.<sup>40,41</sup> Alignments were visualized and interrogated using the Integrative Genomics Viewer v2.3.80.<sup>42</sup>

### Flow cytometry

Cells were harvested with 0.01 M EDTA/PBS, blocked with human IgG (0.1 mg/ml in RPMI media (Life Technologies), 10% fetal bovine serum (FBS, Hyclone, Logan, UT, USA), 0.1% sodium azide (Thermo Fisher Scientific, Waltham, MA, USA) for 10 min on ice prior to staining with an antibody master mix (CD44-PECy7, CD62P-APC, CD62E-APC, ICAM1-PE, ICAM2-APC, VCAM1-FITC, JAMA-PE (all BD), JAMC-VioBright FITC (Miltenyi Biotec, Bergisch Gladbach, Germany)) or the respective isotype controls (IgG2-PECy7, IgG1-APC, IgG1-PE, IgG1-FITC (all BD Biosciences, Franklin Lakes, NJ, USA), REA Control VioBright FITC (Miltenyi Biotec)) with viability dye 7-AAD (BD) in RF10 at manufacturer's recommended concentrations for 30 min, 4°C in the dark. Cells were washed, fixed with FACS fix (PBS with 1% paraformaldehyde, 20 g/L glucose and 5 mM sodium azide (all Sigma-Aldrich, St Louis, MO, USA)) and analyzed on the C6 Accuri™ flow cytometer (BD) using the CFlow® Plus software (BD Biosciences) and FCS Express 4 Flow Cytometry: Research Edition software (De Novo, Pasadena, CA, USA).

In similar experiments, ECFCs and C32 melanoma cells were treated without or with 50 ng/ml VEGF-A (Sigma) for 72 h with the final 24 h including (or not) 10 ng/ml TNF $\alpha$  (R&D Systems). Cells were then assessed for cell surface expression of ICAM-1 and cell viability as detailed above.

### Collection of melanoma cell culture supernatant for chemokine array

Melanoma cell lines were grown to 100% confluency in RF10 prior to replacing the media and culturing cells for a further 3 days. The conditioned media was collected, centrifuged to exclude any cells, filtered with a Minisart 0.2  $\mu$ m syringe filter (Sartorius AG, Gottingen, Germany) and stored at -80°C prior to 1 ml being added to the Proteome Profiler Human Chemokine Array Kit (R&D Systems, Minneapolis, MN, USA). The membrane was visualized using the LAS-4000 (FujiFilm, Tokyo, Japan). Quantification of the dots on the membrane was performed using ImageQuant™ TL (GE Healthcare Life Sciences, Marlborough, MA, USA).

### Microfluidic – parallel plate flow chamber assay

Cells were seeded (and cultured) in 35×10 mm dishes (Corning, Corning, NY, USA) until a confluent monolayer was formed. TrHBMEC cells were treated without or with 50 ng/ml TNF $\alpha$  (R&D Systems) for 4 h prior to the assay. To isolate bulk mononuclear cells (MNC), buffy coats

were diluted 1:1 in PBS, layered onto Lymphoprep™ (Axis-Shield, Dundee, UK) and subjected to gradient centrifugation at 685×g for 20 min with no brake. The MNC layer was collected and washed twice using HUVE wash (M199 supplemented with 2% FBS, 2% 1 M HEPES and 1x Penicillin Streptomycin (Gibco, Thermo Fisher Scientific). Whenever present, red blood cells were lysed using ACK lysis buffer for 5 min and neutralized using HUVE wash. The MNCs were stained with Calcein AM fluorescent dye (1.25 ng/ $\mu$ l in RF10; eBioscience, Thermo Fisher Scientific) for 20 min at RT, washed and resuspended in Hanks' Balanced Salts Solution (HBSS; Sigma-Aldrich) at 4×10<sup>6</sup> cells/ml.

Microfluidic assays were performed using a circular flow chamber kit (GlycoTech Corporation, Gaithersburg, MD, USA), equipped with a 0.01 inch width silicon gasket with 10 mm channel width, and attached to an NE-1000 syringe pump (New Era, Farmingdale, NY, USA) via 1.6 mm internal diameter PharMed tubing (Bio-Rad, Hercules, CA, USA). HBSS and cells at RT were flowed across the monolayer at a flow rate of 0.323 ml/min to achieve a shear stress of 0.5 dynes/cm<sup>2</sup>.

The cell containing dishes were first rinsed with HBSS under flow for 2 min prior to 8×10<sup>6</sup> Calcein AM-stained MNCs flowed across the cell monolayer (flowing 4×10<sup>6</sup> cells/ml at 0.323 ml/min for 6 min 20s), rinsed with HBSS for 6–8 min to remove all unbound cells and adhered labelled MNCs captured using the EVOS® FL Cell Imaging System, a 4x objective, and non-overlapping central fields of view (FOV) captured.

All cells within the dishes were then detached via 0.01 M EDTA/PBS and phenotype determined via flow cytometry. First, cells were blocked with human IgG1 then stained with a master mix in RF10 media (CD3-APC-eFluor780, CD4-PE, CD8-PECy7, CD14-APC, CD16-BV421, CD19-PECy5 (all BD)) or the respective isotype controls (IgG1-APC-eFluor780, IgG1-PE, IgG2-PECy7, IgG1-APC, IgG1-BV421, IgG1-PECy5 (all BD)) with Fixable Viability Stain 700 (BD) for 30 min at 4°C in the dark. Cells were washed and fixed as described above. CountBright™ Absolute Counting Beads (50  $\mu$ l, Life Technologies) were added to the fixed cell sample determine absolute cell counts with samples run on an LSR Fortessa (BD) using FACS Diva Software version 8.0 (BD).

For ICAM-1 knockdown experiments, C32 melanoma cells (at 60%-70% confluency) were transfected with 10 nM 'Trilencer-27' siRNA duplexes from one of three different ICAM-1 targeting sequences (OriGene Technologies, Rockville, MD, USA) via Lipofectamine® RNAiMAX (Invitrogen, Waltham, MA, USA) according to the manufacturer's instructions. Transfection efficiency was verified at 72 h via flow cytometry using ICAM-1-APC or IgG1-APC (both BD) in HUVE media.

To isolate CD14+ monocytes, 10<sup>7</sup> MNCs were resuspended in 90  $\mu$ l of MACS buffer (PBS, 0.5% BSA (Sigma-Aldrich), 2 mM EDTA (Sigma-Aldrich)) together with 10  $\mu$ l of anti-CD14 microBeads (Miltenyi Biotec) for 15 min on ice. Cells were washed with MACS buffer and

resuspended  $<2 \times 10^8$  cells/ml in MACS buffer prior to isolation via the autoMACS separator (Miltenyi Biotec) according to the “possels” program in the manufacturer’s instructions. Sorted cells were rested overnight in DMEM (Life Technologies) supplemented with 10% FBS before use. CD14 expression and cell viability was validated by flow cytometry using CD14-PE or IgG1-PE (both BD) in HUVE media immediately prior to use. Isolated monocytes were stained with Vybrant CFDA SE Cell Tracer Kit (1:1000 dilution, Life Technologies) for 7 min at 37°C before washing with media, resuspending in HBSS at  $4 \times 10^5$  cells/ml and used in the microfluidic assays (as above) with  $\sim 8 \times 10^5$  CD14+ CFDA SE labelled monocytes flowed across the melanoma monolayer.

Selected flow chamber wells were fixed with 4% formaldehyde solution in PBS (Santa Cruz Biotechnology, Dallas, TX, USA) in preparation for scanning electron microscopy.

### Scanning electron microscopy

Cell containing dishes were dehydrated (80% EtOH 24 h, 90% EtOH 24 h, 100% EtOH 24 h, a 50:50 solution of 100% EtOH and Hexamethyldisilazane (Sigma-Aldrich) for 20 min and finally 100% Hexamethyldisilazane for 20 min prior to air drying) prior to the cell region being cut out and coated with platinum (10 nm thickness) in a Cressington 208 HR sputter coater (Cressington, Watford, UK) using an Argon (BOC, North Ryde, NSW, Australia) plasma and platinum sputter target (ProSciTech, Thuringowa Central, Qld, Australia). Samples were examined under a Crossbeam 540 scanning electron microscope with GEMINI II column (Carl Zeiss, Oberkochen, Baden-Wurtemberg, Germany) equipped with a field emission gun operated at 3 kV, a 100 pA probe current applied and secondary electron images recorded with an Inlens Secondary Electron detector.

### Transmigration assay

Cells were seeded into gelatin coated 8.0  $\mu$ m pore Transwell® polycarbonate membrane cell culture inserts (Corning) and grown to confluency. Monolayer permeability was assessed via 2000kDa FITC-dextran (1 mg/ml in PBS; Sigma-Aldrich) being added into the top of the Transwell that was placed into a 24 well plate (Falcon, Corning) containing RF10 for 15 min prior to media being collected from the base plate and fluorescence measured using a FLUOstar OPTIMA microplate reader (BMG LABTECH, Ortenberg, Germany). To confirm a cellular monolayer, the cells were stained with 100  $\mu$ l Calcein AM viability dye (1 ng/ $\mu$ l in RF10; eBiosciences) for 20 min at RT, washed, and the monolayer imaged via EVOS® FL Cell Imaging System (Life Technologies). Only confluent monolayers devoid of holes or tears were selected for experimental use.

MNCs ( $8 \times 10^6$  cells/ml in RPMI with 0.1% FBS) were added to the top chambers of Transwells that contained confluent cell monolayers, transferred into 24-well plates

containing 600  $\mu$ l of either RPMI/0.1% FBS (as a control for non-specific migration) or RF10 (for specific FBS-directed migration). MNCs were placed incubated (5% CO<sub>2</sub> at 37°C) for 3 h prior to Transwell removal and the transmigrated MNCs in the bottom chamber collected and phenotypically analysed via flow cytometry (as above).

In similar experiments,  $1.5 \times 10^5$  C32 cells ( $\pm$  siICAM-1, as above) were seeded into the upper chamber of a Transwell for 4 h prior to excess cells being removed.  $5 \times 10^5$  CD14+ monocytes were fluorescently labelled with Fluo-4 AM (Invitrogen, 1  $\mu$ M in DMEM 10% FBS for 30 min at 37°C prior to washing), resuspended in 0.1% FBS containing media prior to being placed into the upper chamber of a Transwell with 10% FBS chemoattractant in the lower chamber and incubated for 3 h. Media in the lower chamber was then collected, transmigrated cells spun down and Fluo4+ monocytes counted via hemocytometer. Results are presented as mean  $\pm$  SEM from  $n = 3$  different biological blood samples for monocyte isolation.

### The Cancer Genome Atlas (TCGA) analysis

The RNA sequencing data from TCGA melanoma dataset<sup>43</sup> was downloaded from the Data Portal at <http://cancergenome.nih.gov/>. Gene expression values were extracted in R using the edgeR package from Bioconductor.

### Tissue Microarray (TMA)

TMA samples were created from 114 FFPE patient melanoma tissues harvested from metastatic (Stage III/IV) melanomas using an Advanced Tissue Arrayer (Chemicon, Temecula, CA, USA). Samples were dewaxed in xylene (2x10 min, Thermo Fisher Scientific), rehydrated in 100% EtOH and washed with PBS (2x5 min) and tap water. Antigen retrieval was performed in pH9 Tris-EDTA buffer in a pressure cooker for 15 min at “high” and 10 min at “medium.” Washed samples were blocked in 10% normal goat serum (NGS in PBS/0.5% BSA) for 45 min and immunohistochemistry performed as published.<sup>32</sup> For immunofluorescence, samples were incubated with rabbit anti-human CD3 (1:200, Invitrogen) and mouse anti-human CD68 (1:100, BD Biosciences) in PBS/2% NGS/0.5% BSA (or isotype controls) at 4°C overnight. Washed samples were incubated in secondary antibodies (goat anti-rabbit AF-488 at 1:500 and goat anti-mouse AF-594 at 1:500 in PBS/2% NGS/0.5% BSA) at RT for 90 min prior to washing and mounted with Prolong Gold +DAPI (Thermo Fisher Scientific).

In a blinded manner, a score was given for each patient core based on the following criteria – for CD31+ vessel scoring per total core area: 0 = no vessels detected, 1 = 1–10 vessels, 2 = 11+ vessels; CD31- PAS+ VM vessel scoring as a % of total core area: 0 = no VM detected, 1 = network coverage of 5–20%, 2 = network coverage of 21–50%, 3 = network coverage of  $\geq 51\%$ ; CD3 + T cells and CD68 + macrophages scoring: 0 = none detected, 1 = scattered cells or one cluster, 2 = a few clusters or lots of scattered cells, 3 = extensive infiltration.

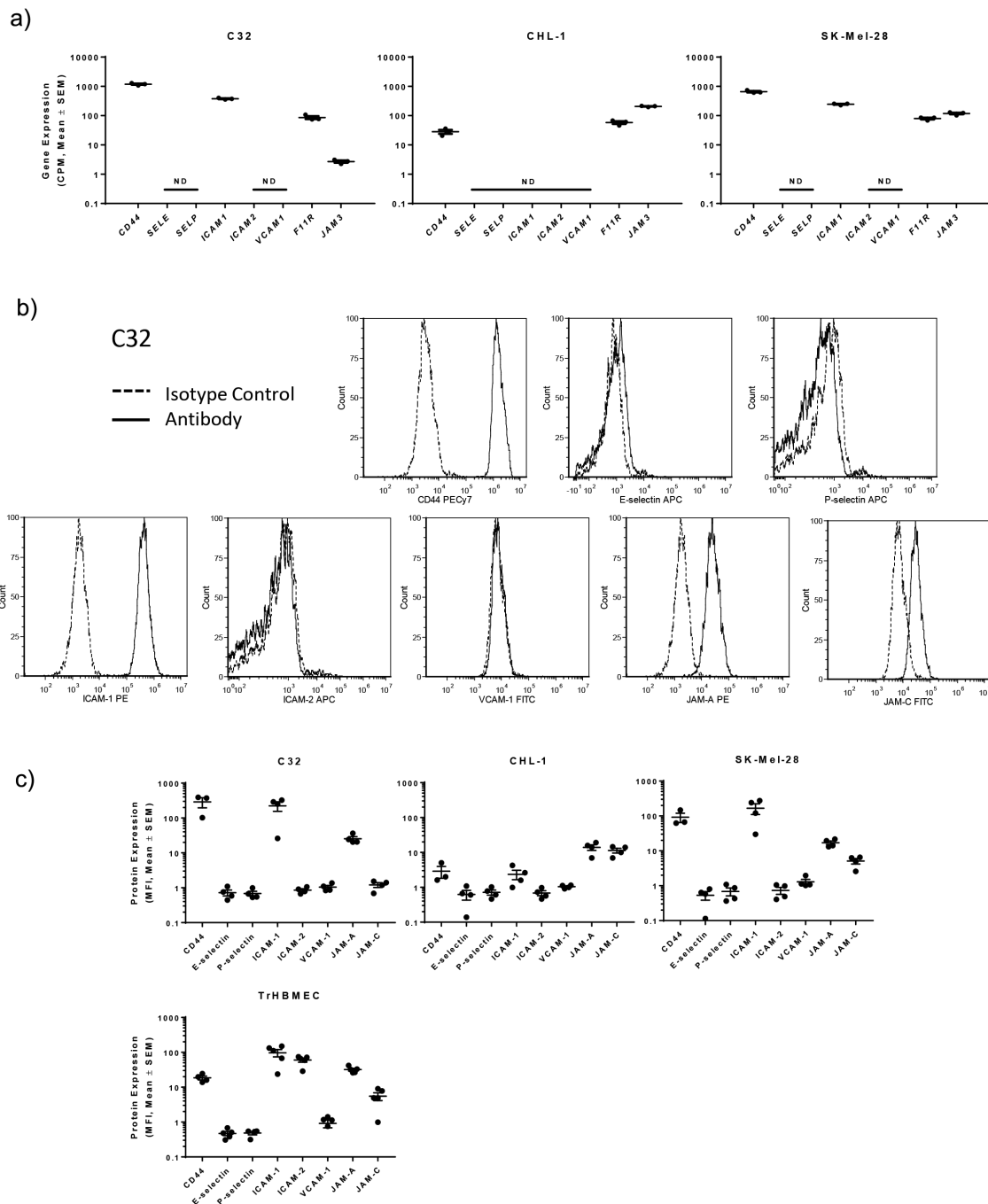


**Figure 1. C32, CHL-1 and SK-Mel-28 express adhesion molecules typically involved in EC leukocyte recruitment.**(a) Dot plots show mean adhesion molecule RNA expression (counts per million, CPM) of melanoma cells cultured under ambient conditions  $\pm$  SEM, with  $n = 3$  independent samples. (b) Representative flow cytometry histograms showing surface protein adhesion molecule expression on C32 cells for  $n = 3$  independent experiments. (c) Dot plots show mean adhesion molecule protein expression (mean fluorescence intensity, MFI) (normalised over isotype control)  $\pm$  SEM, with  $n = 3$ –5 independent experiments.

### Statistical analysis

All statistical analyses were performed using GraphPad Prism software (GraphPad, San Diego, CA, USA). Analyses were performed using two-tailed paired t-tests or one-way repeated measures ANOVA wherever suitable. Bonferroni's Multiple Comparison Test was performed to compare individual groups. Results with  $p < 0.05$  were considered to be statistically significant, with \* =  $p < 0.05$ , \*\* =  $p < 0.01$ , \*\*\* =  $p < 0.001$ .

### Results

#### *VM-competent melanoma cells express adhesion molecules similarly to ECs*

Cancer cells exhibit features of plasticity to enhance their potential for survival, including vasculogenic mimicry. Supplementary Videos 1–3 illustrate the similarities between ECs and C32 melanoma cells to form vascular-

like structures within an *in vitro* tubulogenesis assay while Supplementary Videos 4–5 demonstrate that not all melanoma cells (e.g. M238 cells) exhibit these characteristics.

Given that ECs recruit circulating leukocytes via cell surface expression of adhesion molecules,<sup>7</sup> we examined three VM-competent human melanoma cell lines (i.e. C32, CHL-1 and SK-Mel-28<sup>32</sup>) for their expression of adhesion molecules via an unbiased whole transcriptome RNA sequencing. Following stringent filtering to remove duplicate entries and low level noise (i.e. CPM expression values <1), the filtered data were normalized and revealed robust expression of adhesion molecules by each of the melanoma cell lines. Figure 1A shows that both the C32 and SK-Mel-28 melanoma cell lines expressed mRNA for at least one adhesion molecule required for each step of the leukocyte recruitment cascade, namely *CD44* for leukocyte rolling, *ICAM1* for leukocyte adhesion as well as *F11R* (encodes for JAM-A) and *JAM3* (encodes for JAM-C) required for leukocyte transmigration. In contrast, the CHL-1 cells expressed *CD44*, *F11R*, and *JAM3* but lacked *ICAM1*. Given that VM is, at least in part, activated by hypoxia,<sup>44–47</sup> we also undertook RNA sequencing of the aforementioned cell lines exposed to hypoxic conditions (i.e. 0.5% O<sub>2</sub>) for three or seven days; and with confirmed elevation of hypoxic response genes *BNIP3*, *ENO1*, *LDHA* and *PGK1*<sup>48,49</sup> (Supplementary Figure 1A), we observed that the expression of the adhesion molecules remained largely unchanged (Supplementary Figure 1B).

Next, we assessed protein expression of these adhesion molecules with Figure 1B confirming that the melanoma cells expressed CD44, ICAM-1, JAM-A and JAM-C on their cell surface. Figure 1B illustrates the individual histogram profiles for C32 cell expression of the adhesion molecules while Figure 1C illustrates the mean fluorescence intensity (MFI) for each of the three melanoma cell lines. As expected, the levels of protein expression were comparable to the levels of gene expression and were also largely unchanged under hypoxic conditions (Supplementary Figure 1C). Moreover, Figure 1C also illustrates that the expression of adhesion molecules by these cancer cells was strikingly similar to that of human ECs (TrHBMEC), thus suggesting that VM-competent melanoma cells not only mimic ECs in their formation of vascular structures but also in their expression of leukocyte capturing adhesion molecules.

### **VM-competent melanoma cells express a range of chemokines similar to ECs**

As chemokines and other secreted factors play a crucial role in regulating leukocyte recruitment (reviewed in<sup>6,7</sup>), the RNA sequencing data were further interrogated to study expression of these genes by the three melanoma cell lines. As shown in Figure 2A, the C32, CHL-1 and SK-Mel-28 melanoma cell lines all expressed *CX3CL1*, *CXCL16*, *CCL28*, and *CCL2*; while midkine (*MDK*), *IL16*, *CXCL12*, and *CXCL1* were more restricted. All other chemokine genes investigated were not expressed at detectable levels. We observed no differences in gene expression

in response to hypoxia (Supplementary Figure 2A–B). To validate protein production of these molecules, cell culture supernatants were tested via a commercially available chemokine array. Figure 2B(i) shows that when compared to ‘media alone’, which contained low levels of CXCL12, many other secreted factors were detectable from these VM-competent melanoma cell lines. Densitometric analysis revealed that molecules highly expressed by the VM-competent cell lines include CXCL8 (C32 and SK-Mel-28), CXCL12 (CHL-1), CXCL16 (C32, CHL-1, SK-Mel-28), and midkine (C32, CHL-1). All three cell lines also expressed CX3CL1, albeit at a low level. In addition, SK-Mel-28 cells also expressed lower levels of CCL3/CCL4, CCL20, CXCL1, and CXCL7. Similar levels were detected in the cell culture supernatants following hypoxia (Supplementary Figure 2C). Taken together, these results suggest that VM-competent melanoma cells secrete chemokines and related molecules known to facilitate leukocyte recruitment by ECs.

### **Melanoma cells capture leukocytes under shear flow conditions**

Having confirmed the expression of both adhesion molecules and chemokines typically associated with ECs in mediating leukocyte recruitment, we next asked whether these VM-competent melanoma cells could effectively bind leukocytes under conditions of flow. To address this, we adapted the microfluidic assay to include melanoma cells as the base monolayer traditionally filled by vascular ECs;<sup>50</sup> a schematic is presented as Figure 3A. Briefly, across a confluent monolayer of cells, peripheral blood MNCs were perfused at a flow shear rate documented to exist within a tumor mass (i.e. 0.5 dynes/cm<sup>2</sup>)<sup>51</sup> and identified to firmly adhere via phase contrast microscopy. First, we compared the VM potential of five different human melanoma cell lines against their ability to firmly adhere MNCs under conditions of shear flow. The Matrigel tubulogenesis *in vitro* assay suggests that the MeWo and M238 melanoma lines are VM-incompetent and the microfluidic flow chamber assay suggests that these cancer cells also exhibit a low potential to bind MNCs under shear stress (Figure 3B). In contrast, the melanoma cell lines C32, CHL-1 and SK-Mel-28 exhibited both VM potential and an ability to bind a higher number of the MNCs under flow conditions (Figure 3B). Next, to compare the VM-competent melanoma cells against traditional ECs of the vasculature, we again performed the microfluidic assay. Microscopy images in Figure 3C show the MNCs (labelled with Calcein-AM for ease of viewing) bound to all three VM-competent melanoma cell lines and illustrate that the extent of cell capture was similar to that observed on resting ECs. As expected, MNC adhesion to ECs could be further enhanced following activation by TNF $\alpha$ . To further illustrate that not all cell monolayers can actively bind MNCs under flow conditions, Figure 3C shows that HaCaT keratinocytes capture little-to-no MNCs in this assay. Supplementary Videos 6–8 further support the use of adhesion molecules by VM-competent

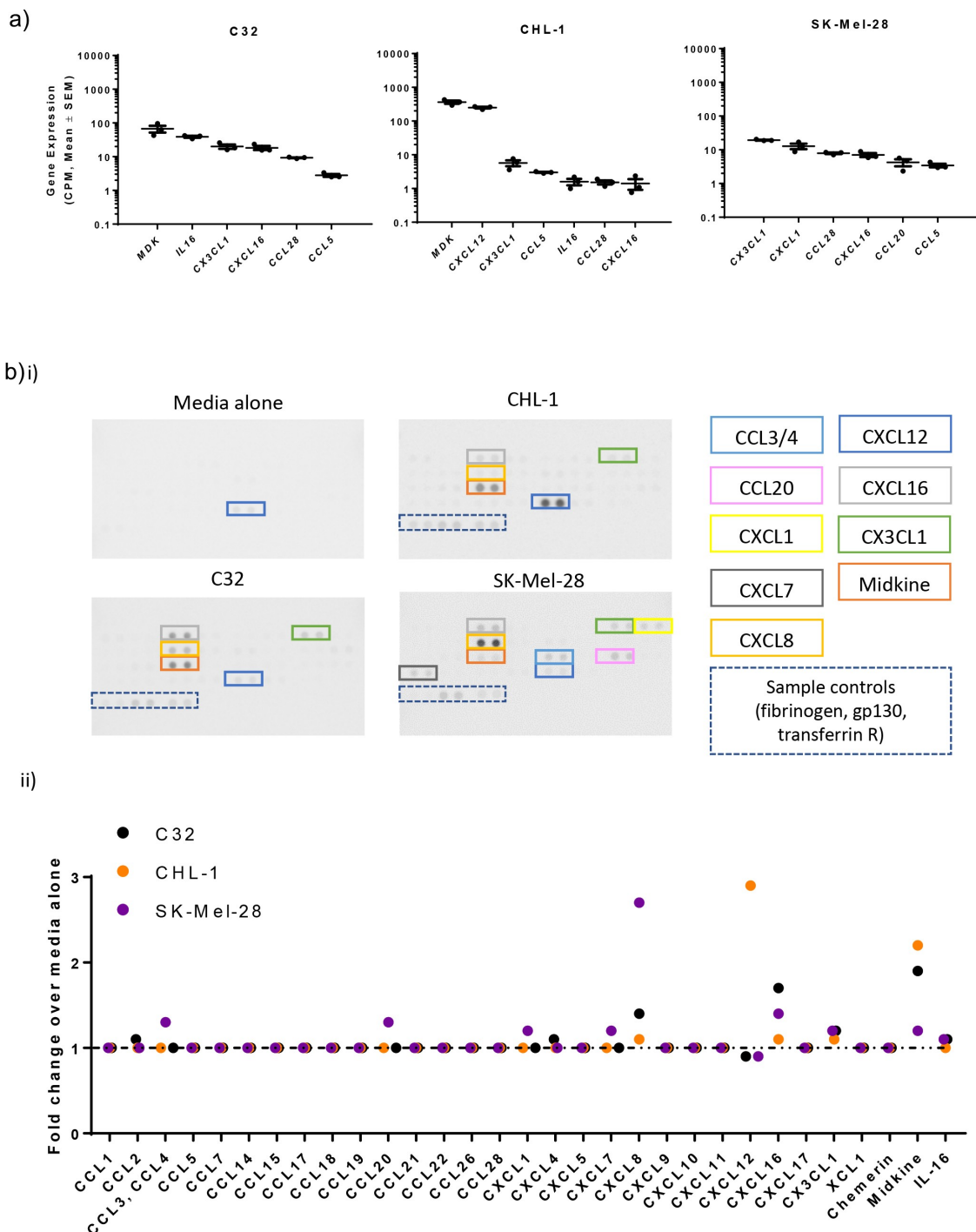


**Figure 2. C32, CHL-1 and SK-Mel-28 express chemokines typically involved in EC leukocyte recruitment.**(a) Dot plots show mean gene expression (counts per million, CPM)  $\pm$  SEM of chemokines expressed by each cell line, with  $n = 3$  independent samples. (b) (i) Chemokine array blots show presence of secreted chemokine protein in cell culture supernatant. For dots that were readily visible on the membrane, the duplicate dots that correspond to different chemokines were boxed and represented with different colours. Dashed box highlight sample controls for the detection of proteins commonly present in cell culture supernatants as a positive control to indicate the sample has been incubated with the array. (ii) Dot plots show chemokines with fold change of corrected pixel intensity over media alone  $> 1$  following subtraction of background with  $n = 1$  experiment.

melanoma cell lines to tether circulating MNCs in rolling actions comparable to those observed on a monolayer of ECs (Supplementary Video 9).

Next, to quantify the number of adherent cells, as well as assess the nature of the leukocytes captured, we detached the cells from the dishes and subjected them to flow cytometric analysis (see Supplementary Figure 3 for gating

strategy). A fixed volume of counting beads was added to each sample to assist in determining the absolute cell numbers. Figure 3D shows that the HaCaT keratinocytes exhibit the lowest number of bound MNCs consistent with their low or absent expression of CD44, ICAM-1 and JAM-A (data not shown). Strikingly, the number of MNCs bound to the VM-competent melanoma cell lines approximated

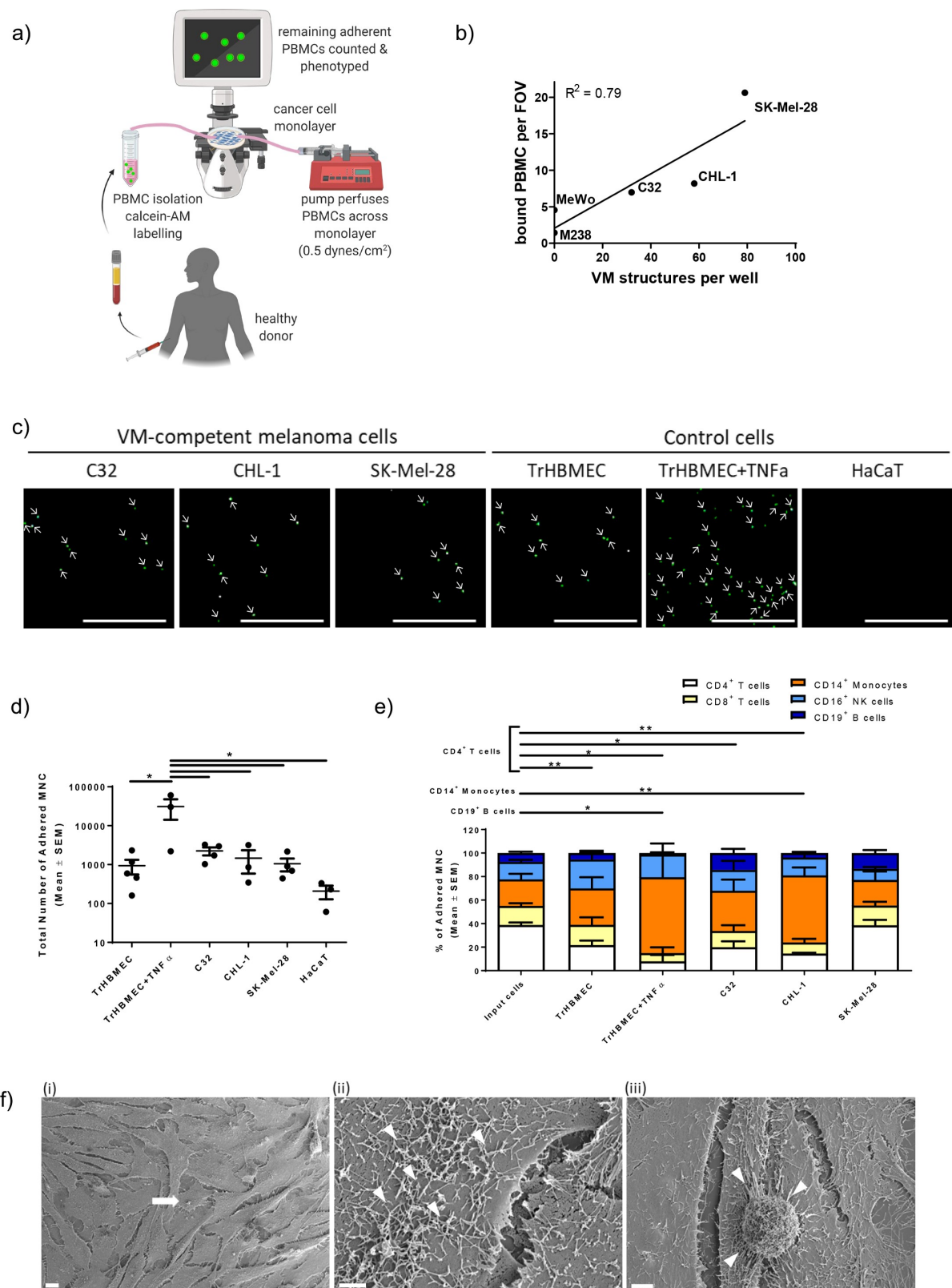


**Figure 3. Leukocytes can adhere on a VM-competent melanoma cell monolayer.** (a) Workflow of microfluidic assays (created with BioRender.com). (b) Melanoma cells lines (SK-Mel-28, CHL-1, C32, MeWo and M238) underwent (i) a Matrigel tubulogenesis assay and VM structures counted per well at 6–8 h post seeding and (ii) a microfluidic assay perfused with PBMC enriched from healthy donors at 0.5 dynes/cm<sup>2</sup> and phase contrast microscopy used to count bound cells per field of view (FOV). Each dot represents an average from 3–11 independent experiments per cell line. A linear regression analysis with 95% confidence intervals was performed for R<sup>2</sup> of the slope. (c) Fluorescence microscopy images taken using a 4x objective showing the adhesion of Calcein AM-labelled MNC on the various cell monolayers prior to detachment for flow cytometric analysis, representative of n = 3–5 independent MNC donors. Scale bars = 400 μm. (d) Dot plot shows the mean total number of adhered MNC on different cell monolayers (deduced following flow cytometric analysis using counting beads) ± SEM with n = 3–5 independent MNC donors. \* = p < 0.05, one way ANOVA with Bonferroni's Multiple Comparison Test. (e) Bar graph shows the mean percentage of different leukocyte subsets within the total population of adhered MNC on different cell monolayers ± SEM with n = 3–5 independent MNC donors. \* = p < 0.05, \* = p < 0.005, two-tailed paired t-test compared to the input population. (f) Representative scanning electron microscopy images showing i) the monolayer of C32 cells with arrow pointing a bound CD14<sup>+</sup> monocyte (scale bar = 10 μm); ii) C32-cell cell junctions with arrowheads showing projections (scale bar = 2 μm); iii) a CD14<sup>+</sup> monocyte bound onto the C32 monolayer under flow conditions (scale bar = 3 μm).



that of ECs (without TNF $\alpha$  stimulation), thus suggesting that VM-competent melanoma cells are functionally similar to resting ECs. To reveal the leukocyte subsets bound, the detached MNCs were stained with a cocktail of fluorescently labelled antibodies to identify CD4 $^{+}$  T cells, CD8 $^{+}$  T cells, CD14 $^{+}$  monocytes, CD16 $^{+}$  NK cells and CD19 $^{+}$  B cells. To determine the final proportion of each cell type as a comparison to the starting population, we also examined the 'input' ratio of leukocyte subsets for each donor prior to use in the assay. Figure 3E shows that the predominant leukocyte subset within the input cells (i.e. peripheral blood MNC) was CD4 $^{+}$  T cells (39%  $\pm$  2%), followed by CD14 $^{+}$  monocytes (23%  $\pm$  5%), CD8 $^{+}$  T cells (16%  $\pm$  2%), CD16 $^{+}$  NK cells (15%  $\pm$  2%) and CD19 $^{+}$  B cells (8%  $\pm$  1%), in keeping with expected frequencies of these cell types in healthy blood.<sup>52</sup> Compared to the input population, the MNCs captured by resting ECs were significantly reduced in the frequency of CD4 $^{+}$  T cells (22%  $\pm$  4%) with a trend towards an increased frequency of CD14 $^{+}$  monocytes (31%  $\pm$  10%). Upon exposure to TNF $\alpha$ , this preferential binding of monocytes over lymphocytes by ECs was further exaggerated with CD14 $^{+}$  monocytes comprising 64%  $\pm$  20%, and CD4 $^{+}$  T cells, 8%  $\pm$  5%, and CD8 $^{+}$  T cells, 1%  $\pm$  11%. Interestingly, we observed a slightly different leukocyte binding profile for each of the three VM-competent melanoma cell lines. For the C32 cells, the overall profile of the leukocyte subsets bound was like that of the EC monolayer, with the bound cells containing significantly fewer CD4 $^{+}$  T cells (19%  $\pm$  5%) and a trend to more monocytes (33%  $\pm$  10%). CHL-1 cells exhibited a leukocyte binding profile similar to that of the TNF $\alpha$ -treated ECs, with a striking enrichment of CD14 $^{+}$  monocytes among the bound cells (57%  $\pm$  7%) compared to the input population. In contrast, the cells recovered from SK-Mel-28 monolayers displayed a similar profile to that of the input cells. The adhesion of CD8 $^{+}$  T cells and CD16 $^{+}$  NK cells was similar across the three VM-competent melanoma cell lines with a possible trend towards less CD19 $^{+}$  B cell binding on the CHL-1 cells.

The aforementioned results suggest that VM-competent melanoma cells preferentially bind monocytes and express adhesion molecules and chemokines known to capture these pro-inflammatory leukocytes. Hence, we undertook scanning electron microscopy (SEM) of C32 cells to view the finger-like cilia projections that are also observed on ECs and are actively involved in leukocyte capture.<sup>53</sup> Figure 3F (i) shows a representative SEM image of a monolayer of C32 melanoma cells on top of which a monocyte has bound. Notably, the dehydration step during sample preparation for SEM caused some contraction of cells leaving gaps at the cell-cell junction and had not been observed by light microscopy during the microfluidic assay. A higher magnification image (Figure 3F (ii)) illustrates that like ECs, C32 cells exhibit a surface covered in cilia. These finger-like projections are known to stretch and attach themselves to leukocytes under flow conditions (Figure 3F (iii)) further supporting their involvement in the process of cell-cell adhesion. Taken together, these

results suggest that VM-competent melanoma cells can mimic a key function of ECs; namely, the active capture of circulating leukocyte subsets under physiologically relevant flow conditions.

### ***ICAM-1 facilitates the adhesion of monocytes to VM-competent melanoma cells***

To further explore the mechanisms facilitating monocyte capture by melanoma cells, similar microfluidic assays were performed using the C32 cells (without and with siRNA-mediated ICAM-1 knockdown) and CD14 $^{+}$  monocytes enriched from the buffy coats of healthy human donors to >90% purity (Figure 4A). Figure 4B shows that compared to the non-targeting siRNA controls, ICAM-1-targeting siRNAs reduce surface expression of ICAM-1 by 45–61% on the C32 cells. Under flow conditions, the number of CD14 $^{+}$  monocytes bound by ICAM-1-deficient C32 cells was reduced significantly by 60–65% (Figure 4 Ci-ii). These experiments suggest that ICAM-1 is an important adhesion molecule used by melanoma cells to bind circulating monocytes. To investigate whether the poor PBMC binding under flow conditions by VM-incompetent MeWo and M238 melanoma cell lines (shown previously in Figure 3B) could be explained by reduced expression of ICAM-1, flow cytometric analysis was performed and revealed levels of ICAM-1 comparable (albeit somewhat lower) to the VM-competent lines C32 and SK-Mel-28 (Supplementary Figure 4). Taken together, these results suggest that ICAM-1 expression by melanoma cells is not restricted to those that can undergo VM. However, in cells that are VM-competent and can bind monocytes, ICAM-1 is required for this adhesion capacity.

### ***Melanoma cells facilitate leukocyte transmigration***

Leukocytes must transmigrate through EC-lined blood vessels to gain access to the underlying tumor mass and exert their functions.<sup>7</sup> To examine whether VM-competent melanoma cells facilitated leukocyte transmigration, we performed Transwell migration assays (schematic shown in Figure 5A). First, melanoma cells were seeded into the upper chamber of Transwell dishes and then stained with Calcein-AM to confirm that a confluent monolayer of cancer cells had formed (Figure 5B). All Transwells with areas lacking Calcein-AM stained cells were discarded. Next, we examined the permeability of the monolayers by loading high molecular weight (2000 kDa) FITC-dextran into the top chamber and measuring levels passing to the lower chamber after 15 min. Figure 5C shows that control Transwells (without a monolayer of cells) exhibited the highest levels of FITC-dextran whereas the HaCat keratinocytes demonstrated the strongest barrier integrity, with the lowest detectable levels of FITC-dextran. Although cells of the C32, CHL-1 and SK-Mel-28 melanoma cell lines were more permeable to FITC-

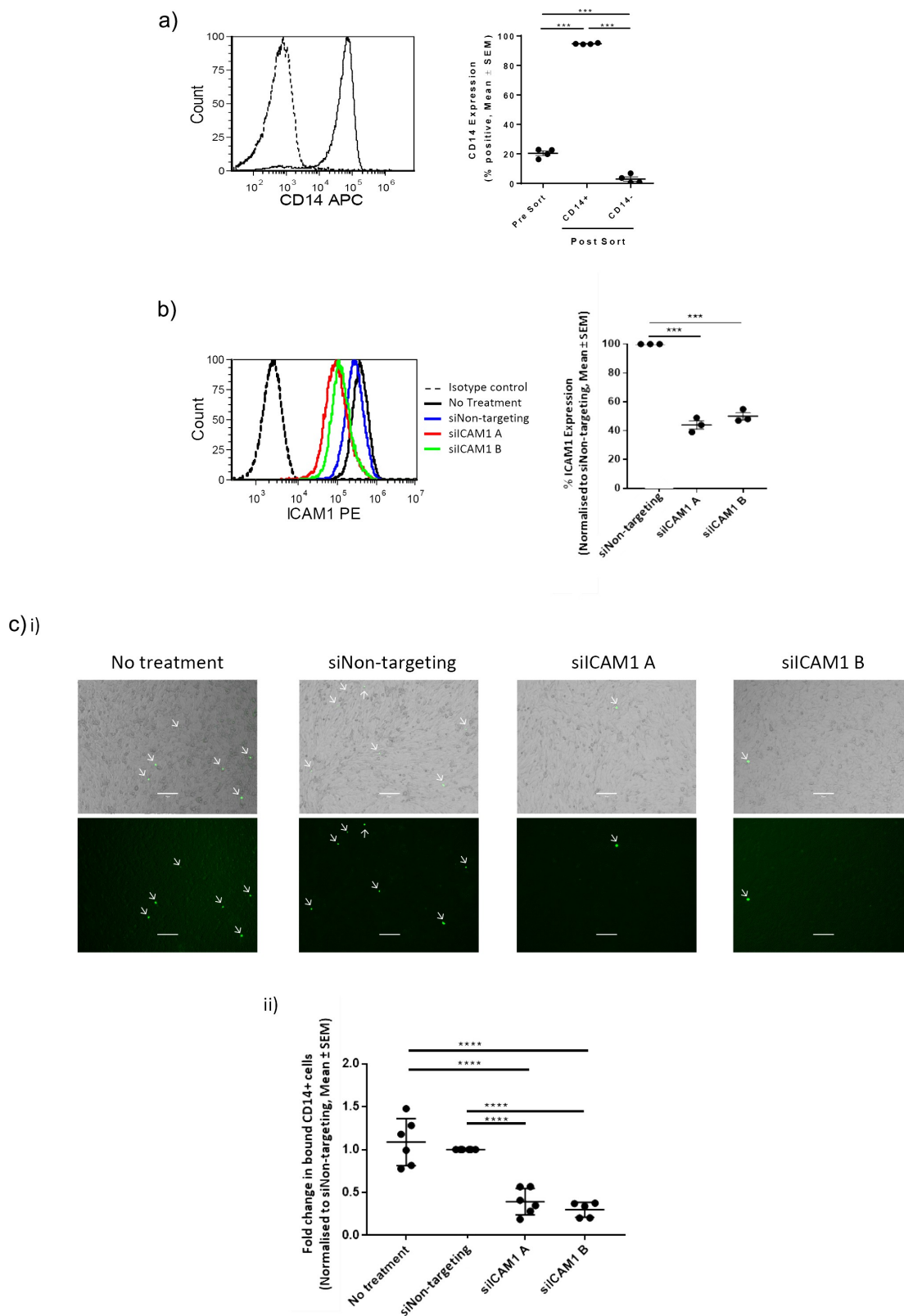


**Figure 4. The adhesion of monocytes on C32 cells is partly mediated by ICAM-1.** (a) Representative histogram showing CD14<sup>+</sup> cells (solid line) compared to isotype control (dashed). Dot plot shows quantified CD14<sup>+</sup> purity for  $n = 4-5$  independent MNC donors. \* =  $p < 0.05$ , \*\* =  $p < 0.01$ , two-tailed paired t-test. (b) Representative flow cytometry histogram showing surface ICAM-1 expression levels on C32 cells under various treatments, with dot plot showing mean ICAM-1 expression (normalised to non-targeting siRNA control)  $\pm$  SEM for  $n = 3$  independent transfections. \* =  $p < 0.05$ , \*\* =  $p < 0.01$ , two-tailed paired t-test compared to the non-targeting siRNA control. (c) (i) Fluorescence microscopy images showing the adhesion of CFSE labelled CD14<sup>+</sup> monocytes on the various cell monolayers following microfluidic assays, representative of  $n = 4$  independent MNC donors. Scale bar = 20  $\mu$ m. (ii) Dot plot shows the mean number of CD14<sup>+</sup> monocytes adhered  $\pm$  SEM with  $n = 4$  independent MNC donors. \* =  $p < 0.05$ , \*\* =  $p < 0.01$ , two-tailed paired t-test.

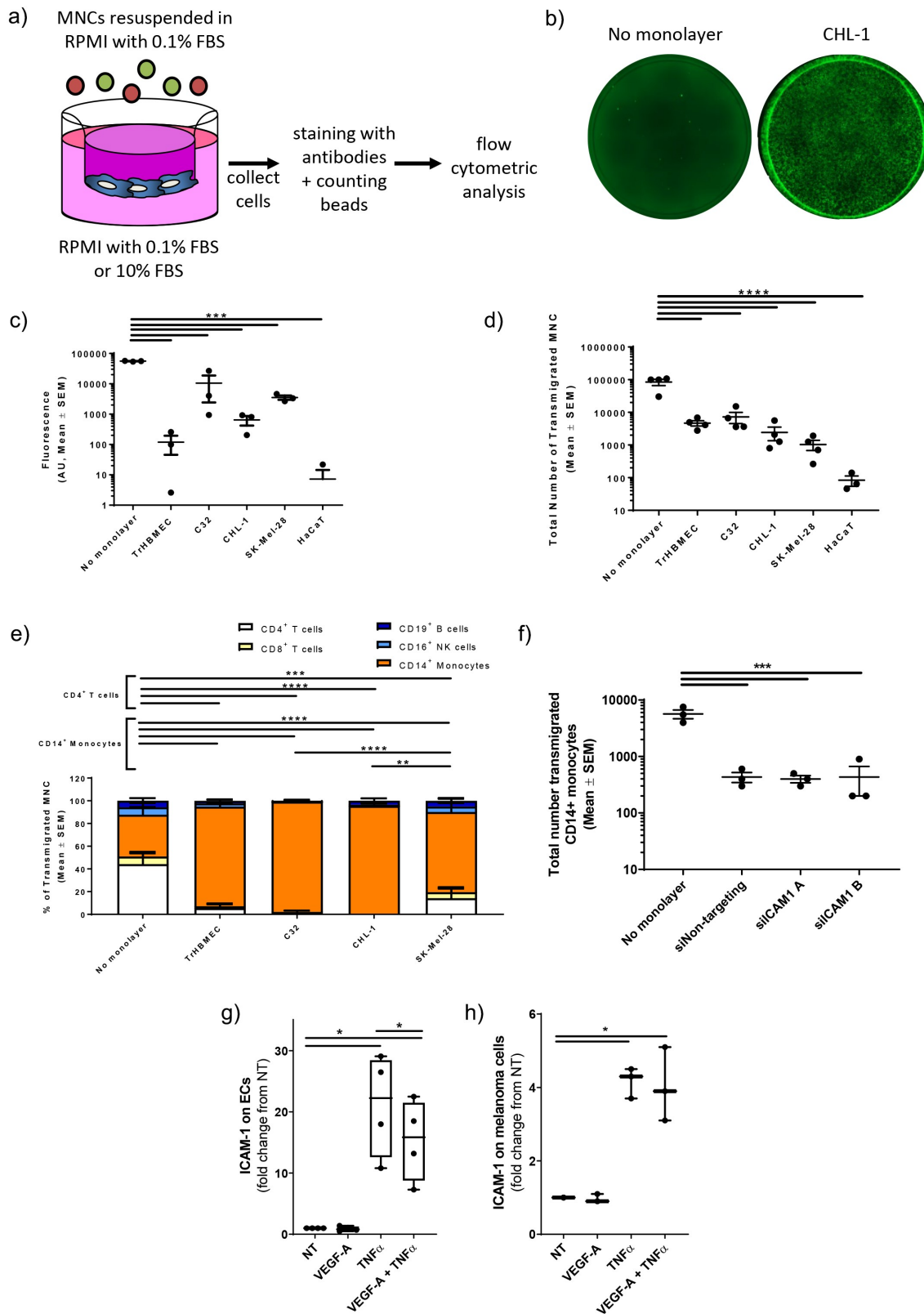


**Figure 5. VM-competent melanoma cells are selectively permissive towards monocyte transmigration.** (a) Figure showing setup and workflow of Transwell assays. (b) Representative images showing staining for Transwells with no monolayer and CHL-1 with  $n \geq 3$  independent experiments. (c) Dot plot shows the mean fluorescence in arbitrary units for each of the different monolayers (reflective of monolayer permeability to 2000 kDa FITC-dextran)  $\pm$  SEM from  $n = 3$  independent experiments. \*\*\* =  $p < 0.001$ , one-way ANOVA with Bonferroni's Multiple Comparison Test. (d) Dot plot shows the mean total number of transmigrated MNC for all the different cell monolayers (deduced following flow cytometric analysis using counting beads with any non-specific migration deducted)  $\pm$  SEM from  $n = 4$  independent MNC donors. \*\*\*\* =  $p < 0.0001$ , one-way ANOVA with Bonferroni's Multiple Comparison Test. (e) Bar graph shows the mean chemotactic differentials for the different leukocyte subsets for each of the cell monolayers  $\pm$  SEM with  $n = 4$  independent MNC donors. \* =  $p < 0.05$ , \*\* =  $p < 0.005$ , two-tailed paired t-test. (f) Dot plot shows the mean total number of transmigrated CD14<sup>+</sup> monocytes  $\pm$  SEM from  $n = 3$  independent donors. \*\*\* =  $p < 0.001$ , one-way ANOVA with Bonferroni's Multiple Comparison Test. (g) Fold change in ICAM-1 mean fluorescence intensity relative to untreated (NT) ECs and in response to VEGF-A (50 ng/ml, 72 h) without or with TNF $\alpha$  (10 ng/ml, 24 h). Dots represent individual experiments  $\pm$  SEM from  $n = 4$  independent donors. # =  $p < 0.05$  one-way ANOVA with Bonferroni's Multiple Comparison Test. \* =  $p < 0.05$ , paired t-test. (h) Fold change in ICAM-1 mean fluorescence intensity relative to untreated (NT) melanoma cells and in response to VEGF-A (50 ng/ml, 72 h) without or with TNF $\alpha$  (10 ng/ml, 24 h). Dots represent individual experiments  $\pm$  SEM from  $n = 3$  independent experiments. # =  $p < 0.05$  one-way ANOVA with Bonferroni's Multiple Comparison Test.

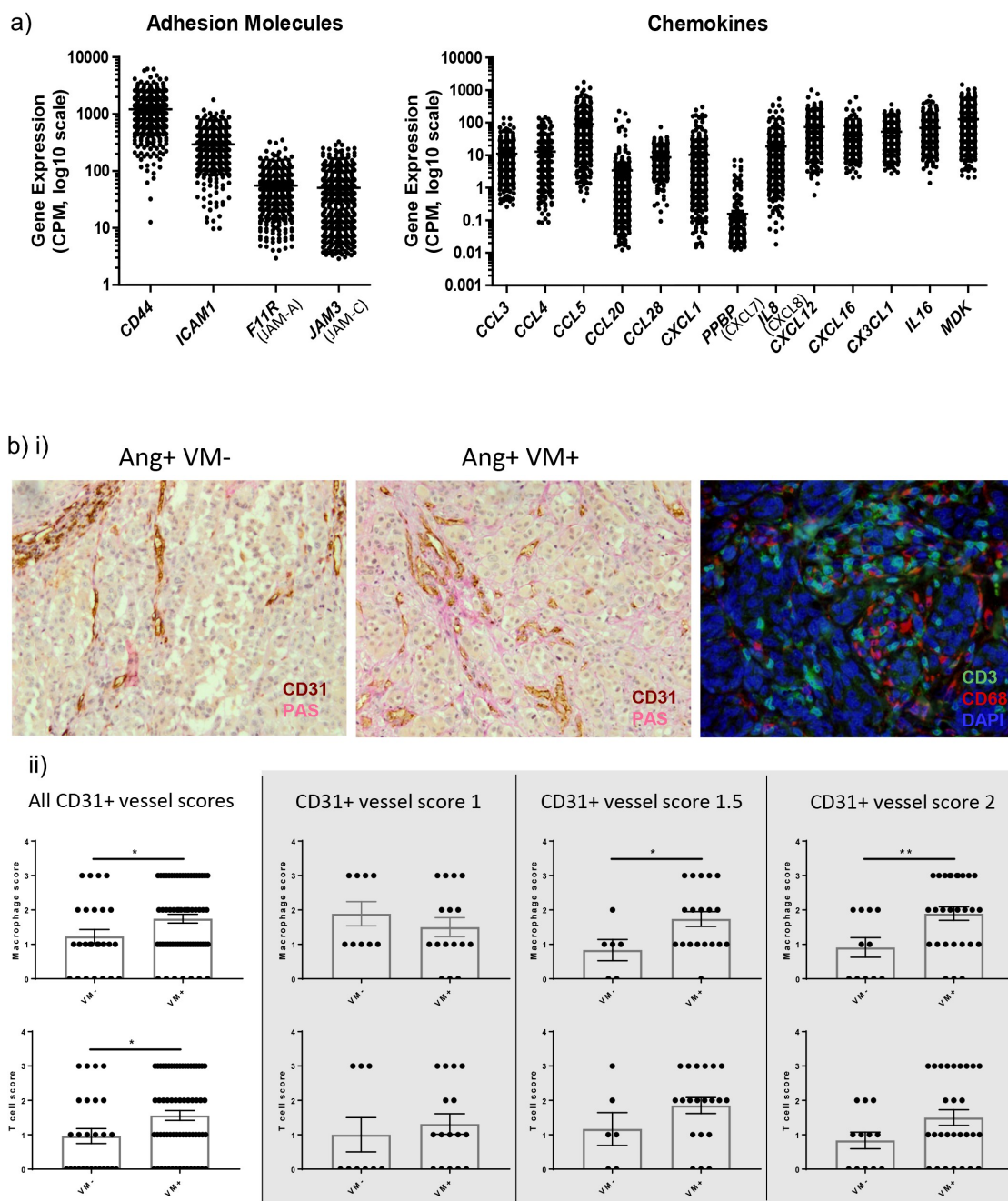


**Figure 6. In silico TCGA gene expression analysis of adhesion molecules and chemokines and TMA immunofluorescence showing VM and infiltration of T cells and macrophages.** (a) Dot plots show the gene expression (CPM, log<sub>10</sub> scale) of the different adhesion molecules and chemokines for n = 427 samples in The Cancer Genome Atlas (TCGA) melanoma dataset. (b) Representative immunohistochemistry images showing CD31+ conventional blood vessels and CD31- PAS+ VM vessels, as well as representative immunofluorescence images showing CD68+ macrophages and CD3+ T cells in human melanoma tissue microarrays. Dot plots show mean scores of macrophages or T cells under different CD31+ vessel scores ± SEM with n = 25–39 duplicate cores. \* = p < 0.05, \*\* = p < 0.005, two-tailed unpaired t-test.

dextran than the EC monolayer, the cancer cells consistently formed an effective barrier when compared to the no monolayer control.

Having confirmed that the melanoma cells form a physical barrier, we performed Transwell assays using fetal bovine serum (FBS) as a chemoattractant (0.1% in the upper well and 10% in the lower chamber). Control Transwells without an FBS gradient (i.e. 0.1% to 0.1%) were also included to quantify any nonspecific migration. Results were determined as a ‘chemotactic differential’ by subtracting the number of cells that migrated in the

absence of an FBS gradient from those that migrated across the monolayer and towards the 10% FBS gradient. As expected, the control Transwells, which contained no cellular barrier, showed the highest number of transmigrated MNCs (Figure 5D). In contrast, the HaCaT keratinocytes were largely non-permissive to leukocyte transmigration, with almost no MNCs migrating across the monolayer. Of note, monolayers formed from each of the three VM-competent melanoma cell lines permitted the migration of significantly more leukocytes than was observed for HaCaT containing Transwells, and at times, equivalent to the

ECs (Figure 5D). Together, the three melanoma cell lines analyzed suggest a permissive capacity for monocyte transmigration, a potentially important feature for the promotion of an immunosuppressive phenotype. Investigating this further will be aided by an *in vivo* comparison of melanoma VM potential, ICAM-1 expression, monocyte transmigration and metastatic potential.

Next, we used flow cytometry to identify the leukocyte subsets that transmigrated through the cancer cells monolayers. Figure 5E shows that the MNCs collected from control wells (no monolayer) comprised CD4+ T cells (44% ± 11%), CD8+ T cells (7% ± 3%), CD14+ monocytes (37% ± 7%), CD16+ NK cells (7% ± 4%) and CD19+ B cells (6% ± 2%), indicating that all five leukocyte subsets are responsive to the FBS gradient. In the presence of an EC monolayer, we observed a significant enrichment of CD14+ monocytes (88% ± 6%) and a reduction in CD4+ T cells (to 6% ± 4%). Similar to the EC monolayer, all three VM-competent melanoma monolayers influenced transmigration with CD14+ monocytes exhibiting a higher rate of migration (i.e. C32: 97% ± 2%, CHL-1: 96% ± 3%, SK-Mel-28: 71% ± 12%) than the CD4+ T cells- (i.e. C32: 2% ± 1%, CHL-1: 0%, SK-Mel-28: 14% ± 10%).

To investigate whether a role for ICAM-1 extends beyond cell adhesion and through to active transmigration, similar chemotaxis assays were performed using the C32 cells (without and with siRNA-mediated ICAM-1 knockdown) and CD14+ monocytes. As expected, Figure 5F shows that knockdown of ICAM-1 did not influence monocyte transmigration towards the chemoattractant.

Finally, with documentation that prolonged exposure of tumor ECs to VEGF-A renders these cells anergic through reduced expression of adhesion molecules, including ICAM-1,<sup>9,10</sup> we investigated whether this response is also a feature of VM-competent melanoma cells. First, Figure 5G shows that TNF $\alpha$  increases expression of ICAM-1 on ECs and that this response is dampened when the ECs are pre-exposed to VEGF-A. In contrast, while the VM-competent C32 melanoma cells do respond

to TNF $\alpha$  with increased expression of ICAM-1, this response is not dampened by pre-treatment with VEGF-A (Figure 5H).

Taken together, these results suggest that VM-competent melanoma cells are remarkably similar to ECs in terms of preferential recruitment of myeloid cells, but potentially different in their retention of ICAM-1 expression following prolonged exposure to the tumor microenvironment milieu.

### Clinical melanoma tissues express adhesion molecules and chemokines

Having established the ability of VM-competent human melanoma cells to mediate leukocyte adhesion and transmigration *in vitro*, we next examined the relevance of this phenomenon in human tumor samples. First, we performed an *in silico* analysis of The Cancer Genome Atlas (TCGA) melanoma dataset<sup>43</sup> to determine whether human patient melanomas also expressed the aforementioned adhesion molecules and chemokines. Figure 6A shows the abundant expression of adhesion molecules *CD44*, *ICAM1*, *F11R* (JAM-A), *JAM3* (JAM-C) and chemokines by the patient samples. As TCGA gene expression analysis was performed from whole tumor samples, which also contain stromal tissue (e.g. ECs), we performed a correlation study to examine if the detected expression of adhesion molecules and chemokines was associated with EC abundance. To do this, we compared gene expression levels against the expression of endomucin (*EMCN*, a key marker of ECs<sup>54</sup>), as well as microphthalmia-associated transcription factor (*MITF*, a melanoma cell lineage marker)<sup>55</sup> Table 1 shows that the correlation coefficients for the majority of the genes were small (between -0.1 and 0.1), thus suggesting that the expression of these genes could not clearly be attributed to either ECs or melanoma cells. Overall, of all the genes examined, the top two positive correlation coefficients were between *MITF* and *CCL28* (0.4342) as well as *MITF* and *CD44* (0.31) (Table 1, green highlight), suggesting that the expression of these molecules is largely contributed by melanoma cells and not ECs. Interestingly, we observed *CCL28* to be significantly elevated in response to hypoxia in the CHL-1 cells with a similar trend observed in the C32 and SK-Mel-28 cells (Supplementary Figure 2A).

**Table 1.** Summary of correlation analysis performed to examine the correlation of adhesion molecule and chemokine expression of TCGA samples with EC frequency (*EMCN*) and melanoma frequency (*MITF*).

Gene	Correlation with <i>EMCN</i>		Correlation with <i>MITF</i>	
	Spearman's r	p-value	Spearman's r	p-value
<i>CD44</i>	-0.0517	0.2860 (n.s.)	0.3136	<0.0001
<i>ICAM1</i>	-0.1960	<0.0001	-0.0465	0.3382 (n.s.)
<i>F11R</i>	-0.1164	0.0161	0.1946	<0.0001
<i>JAM3</i>	0.2111	<0.0001	-0.2833	<0.0001
<i>CCL3</i>	-0.0634	0.1910 (n.s.)	-0.1182	0.0145
<i>CCL4</i>	-0.0154	0.7508 (n.s.)	-0.1515	0.0017
<i>CCL5</i>	-0.0379	0.4650 (n.s.)	-0.1611	0.0008
<i>CCL20</i>	-0.1972	<0.0001	-0.1551	0.0013
<i>CCL28</i>	-0.1845	<0.0001	0.4342	<0.0001
<i>CXCL1</i>	-0.3461	<0.0001	0.0363	0.4546 (n.s.)
<i>PPBP</i>	0.0957	0.0480	-0.1108	0.0220
<i>IL8</i>	-0.1195	0.0135	-0.1134	0.0191
<i>CXCL12</i>	0.2481	<0.0001	-0.1915	<0.0001
<i>CXCL16</i>	0.0109	0.8220 (n.s.)	-0.3328	<0.0001
<i>CX3CL1</i>	-0.1883	<0.0001	0.0655	0.1764 (n.s.)
<i>IL16</i>	-0.1757	0.0003	0.1120	0.207
<i>MDK</i>	0.1330	0.0059	-0.2962	<0.0001

n.s. = non significant

### Presence of VM vessels in human melanoma tissues correlates with increased macrophage numbers

To investigate a correlation between VM content, EC content and leukocyte infiltration within tumor samples, we performed immunostaining on human melanoma tissue microarrays (TMAs). The array contained 114 human metastatic melanoma specimens (each with duplicate cores) that were stained for tumor vasculature using anti-CD31 (to mark ECs) and Periodic acid Schiff (PAS, that labels basement membrane collagens and laminins). This enables EC-lined vessels to be identified as CD31+/PAS+ and VM structures to be identified as CD31-/PAS+.<sup>26</sup> In contiguous TMA sections, immunofluorescence staining was performed for CD3+ T cells and CD68+ macrophages. Figure 6B(i) illustrates an example of tumor samples that

are VM-, VM+ and that contain CD3+ T cells and CD68+ macrophages. In a blinded manner, a score was given for each patient core based on stringent criteria as described in the Materials and Methods section. Results were presented as the average score from duplicate cores. As shown in Figure 6B(ii), when the tumors were separated into VM- (score = 0) and VM+ (scores  $\geq 1$ ) groups, the VM+ tumors expressed a significantly higher CD68+ macrophage score as well as a significantly higher CD3+ T cell score. Further analysis of groups based on the abundance of CD31+ blood vessels (i.e. scores of 1, 1.5 or 2) revealed that the link between VM and macrophage frequency was most prominent in highly vascularized tumors, where VM+ tumors exhibited a greater increase in CD68+ macrophages than the VM- tumors. Taken together, these observations based on human patient samples support our *in vitro* findings and our hypothesis that VM-competent melanoma cells actively participate in the recruitment of leukocytes (particularly myeloid cells) into solid tumors.

## Discussion

The direct formation of vascular structures by aggressive cancer cells such as melanoma was first reported in 1999<sup>56</sup> and since then has significantly contributed to our understanding of cancer.<sup>22</sup> Advanced scientific techniques confirmed that VM vessels are perfused with active blood flow<sup>19–21</sup> and contribute to increased tumor growth *in vivo*.<sup>24,25</sup> More importantly, VM is frequently detected in solid cancers and is particularly associated with disease aggressiveness and poor prognosis.<sup>26,27</sup> VM vessels share many features with EC-lined vessels, including their induction in response to hypoxia via the VEGF-A/VEGFR/PI3K pathway<sup>45–47</sup> and their upregulation of the anti-coagulative tissue factor pathway inhibitor (TFPI).<sup>21</sup>

Herein, we present new data suggesting that VM-competent melanoma cells actively mediate a key function of ECs; leukocyte recruitment. We show that VM-competent melanoma cell lines express a suite of adhesion molecules and chemokines that equip them for the selective capture, adhesion and transmigration of circulating leukocytes. Most notably, ICAM-1 facilitated the adhesion of CD14+ monocytes on VM-competent melanoma cells. Curiously, very few, if any, adhesion molecules and chemokines expressed by the melanoma cells were altered in response to 3–5 days of hypoxia. We observed cilia-like protrusions on the VM-competent melanoma cells, similar to those identified on ECs and involved in leukocyte capture.<sup>53</sup> Finally, our patient tissue data demonstrate a correlation between an increase in VM vessels and intratumoral levels of macrophages and T cells. Together, these observations support our hypothesis that VM vessels promote tumor growth via their selective control of leukocyte subsets that enter the tumor microenvironment from the bloodstream. We contend that VM vessels actively recruit monocytes into the tumor mass to promote their maturation into pro-tumorigenic M2 macrophages,<sup>57</sup> which can occur independently of an anergic EC-lined tumor vasculature.

Interestingly, despite expressing the adhesion molecules required to mediate T cell recruitment (including ICAM-1 and JAM), we did not observe enhanced T-cell recruitment by VM competent melanoma cells under flow conditions. This can potentially be explained by their chemokine profile. In particular, melanoma cells did not express detectable levels of CXCL9, CXCL10 and CXCL11, which are known to interact with their receptor CXCR3 on T cells. This finding is important because CXCR3 has been reported to play a non-redundant role in controlling CD8+ T cell trafficking to human and murine melanoma and the absence of this signaling axis leads to impaired T cell recruitment and cancer progression.<sup>16</sup> In contrast, all three melanoma cell lines expressed the chemokines CX3CL1 and CXCL16 at the gene and protein level, and expression of these chemokine genes was abundant within patient melanoma tissues. Both CX3CL1 and CXCL16 have been implicated in the recruitment of myeloid cells into tumors,<sup>58,59</sup> and their receptors (CX3CR1 and CXCR6, respectively) are expressed by blood monocytes.<sup>60,61</sup> Interestingly, *CCL28* exhibited the highest correlation coefficient with *MITF* in TCGA human melanoma samples and was the only chemokine to exhibit increased expression in response to hypoxia in all of the melanoma cell lines tested (albeit marginally for the C32 and SK-Mel-28 cells). The role of *CCL28* in melanoma is yet to be fully elucidated, but potential modes of action documented in other cancer types include cancer cell proliferation<sup>62</sup> and tumor associated angiogenesis,<sup>63,64</sup> investigating this further is a future direction of our work. One limitation of our study was to use supernatants from cancer cell cultures to profile the chemokine proteins. It is possible that some chemokine proteins are stored within intracellular granules or exosomes, investigating this further is another future direction of our work.

Our novel finding of an alternative avenue for leukocyte recruitment into tumors has significant implications, particularly for the development of new cancer therapeutics to alter the immune composition of melanoma for sustained tumor destruction. Tumor regression following chemotherapy, low-dose radiation, anti-angiogenic agents, BRAF and MEK inhibitors, with or without immunotherapy has been attributed to the enhanced infiltration of CD8+ T cells.<sup>65–69</sup> For example, Lacial, Graziani and colleagues showed in a mouse model of melanoma that a monoclonal antibody to VEGFR-1 (D16F7) could perturb tumor growth via reduced tumor associated angiogenesis, reduced VM by tumor cells, decreased CD163+ M2 myeloid cell infiltration, but increased CD8+ T cell infiltration and increased anti-tumor activity of immune checkpoint inhibitors.<sup>70,71</sup> Congruent with this is a further study by Straetemans et al demonstrating that relapsed B16 tumors exhibit decreased levels of CD8+ T cells and monocytes in response to prolonged stimulation by VEGF or bFGF which dampen expression of adhesion molecules and chemokines.<sup>72</sup> Our findings support the concept of targeting the tumor milieu, with VM vessels expressing ICAM-1 being an attractive route for therapeutic chimeric antigen receptor T (CAR-T) cells. Ensuring that CAR-T cells

express the counter ligand LFA-1 may help to overcome a current hurdle of T cell exclusion by most solid tumors. Alternatively, if stable ICAM-1 expression on the VM vessels *in vivo* is confirmed to drive the accumulation of TAMs, therapies aimed at preventing the entry of these pro-tumorigenic cells could be developed on the basis of blocking VM formation, or targeting key molecules involved in monocyte recruitment.

Until now, the entry of leukocytes into solid tumors was thought to be controlled exclusively by the ECs that line tumor blood vessels. Here, we propose an additional, pro-tumorigenic mechanism for regulating intratumoral leukocyte traffic, whereby cancer cell-lined VM channels selectively capture leukocytes from the bloodstream and facilitate their passage into tumor tissue. Future studies in mouse models are warranted to confirm these mechanisms *in vivo* because an improved understanding of the formation and function of VM vessels in tumors may lead to the design of new therapies.


## Disclosure statement

No potential conflict of interest was reported by the author(s).

## Funding

This work was supported by an Australian National Health and Medical Research Council project grant to CSB and LME (GNT1164945), a Royal Adelaide Hospital Florey Fellowship to LME, a Royal Adelaide Hospital Clinical Project grant to LME and MPB, a Beat Cancer Hospital Research Package to MPB and AR, a Health Services Charitable Gifts Board funding to MPB, a Cancer Australia grant to LME (GNT1186306) an Australian Government Research Training Program Scholarship to LYT and a Cell Therapy for Manufacturing Co-operative Research Centre scholarship top-up to LYT.

## ORCID

Michaelia P. Cockshell  <http://orcid.org/0000-0002-1350-2988>  
 Eli Moore  <http://orcid.org/0000-0002-4131-8299>  
 Kay K. Myo Min  <http://orcid.org/0000-0002-3747-8556>  
 M. Zahied Johan  <http://orcid.org/0000-0003-3053-8509>  
 Andrew Ruskiewicz  <http://orcid.org/0000-0001-9052-4948>  
 Lisa M. Ebert  <http://orcid.org/0000-0002-8041-9666>  
 Claudine S. Bonder  <http://orcid.org/0000-0001-9875-967X>

## Synopsis

Vasculogenic mimicry by human melanoma cells promotes disease progression. This study shows that VM-competent cancer cells express adhesion molecules and produce chemokines to preferentially recruit monocytes under conditions of shear flow. This is an unexpected finding as until now, the entry of leukocytes into solid tumors was thought to be controlled exclusively by endothelial cell-lined tumor blood vessels.

## References

1. Australian Institute of Health and Welfare, Cancer in Australia Report. 2019.
2. McKay K, Moore PC, Smoller BR, Hiatt KM. Association between natural killer cells and regression in melanocytic lesions. *Hum Pathol.* 2011;42(12):1960–1964. doi:10.1016/j.humpath.2011.02.019.
3. Weishaupt C, Munoz KN, Buzney E, Kupper TS, Fuhlbrigge RC. T-cell distribution and adhesion receptor expression in metastatic melanoma. *Clin Cancer Res.* 2007;13(9):2549–2556. doi:10.1158/1078-0432.CCR-06-2450.
4. Ahmadzadeh M, Felipe-Silva A, Heemskerk B, Powell DJ, Wunderlich JR, Merino MJ, Rosenberg SA. FOXP3 expression accurately defines the population of intratumoral regulatory T cells that selectively accumulate in metastatic melanoma lesions. *Blood.* 2008;112(13):4953–4960. doi:10.1182/blood-2008-06-163048.
5. Torisu H, Ono M, Kiryu H, Furue M, Ohmoto Y, Nakayama J, Nishioka Y, Sone S, Kuwano M. Macrophage infiltration correlates with tumor stage and angiogenesis in human malignant melanoma: possible involvement of TNF $\alpha$  and IL-1 $\alpha$ . *Int J Cancer.* 2000;85(2):182–188. doi:10.1002/(SICI)1097-0215(20000115)85:2<182::AID-IJC6>3.0.CO;2-M.
6. Missiaen R, Mazzone M, Bergers G. The reciprocal function and regulation of tumor vessels and immune cells offers new therapeutic opportunities in cancer. *Semin Cancer Biol.* 2018;52:107–116.
7. Tan LY, Martini C, Fridlender ZG, Bonder CS, Brown MP, Ebert LM. Control of immune cell entry through the tumour vasculature: a missing link in optimising melanoma immunotherapy? *Clin Translation Immunol.* 2017;6(3):e134–e. doi:10.1038/cti.2017.7.
8. Carlos TM. Leukocyte recruitment at sites of tumor: dissonant orchestration. *J Leukoc Biol.* 2001;70:171–184.
9. Dirx AE, Oude Egbrink MG, Kuijpers MJ, van der Niet ST, Heijnen VV, Bouma-ter Steege JC, Wagstaff, J, and Griffioen, AW. Tumor angiogenesis modulates leukocyte-vessel wall interactions *in vivo* by reducing endothelial adhesion molecule expression. *Cancer Res.* 2003;63(9):2322–2329.
10. Hellebrekers DM, Castermans K, Vire E, Dings RP, Hoebers NT, Mayo KH, Oude Egbrink, MG, Molema, G, Fuks, F, and van Engeland, M, et al. Epigenetic regulation of tumor endothelial cell anergy: silencing of intercellular adhesion molecule-1 by histone modifications. *Cancer Res.* 2006;66(22):10770–10777. doi:10.1158/0008-5472.CAN-06-1609.
11. Nooijen PT, Westphal JR, Eggermont AM, Schalkwijk C, Max R, de Waal RM, and Ruiters, DJ. Endothelial P-selectin expression is reduced in advanced primary melanoma and melanoma metastasis. *Am J Pathol.* 1998;152(3):679–682.
12. Piali L, Fichtel A, Terpe HJ, Imhof BA, Gisler RH. Endothelial vascular cell adhesion molecule 1 expression is suppressed by melanoma and carcinoma. *J Exp Med.* 1995;181(2):811–816. doi:10.1084/jem.181.2.811.
13. Clancy-Thompson E, Perekslis TJ, Croteau W, Alexander MP, Chabanet TB, Turk MJ, Huang YH, Mullins DW. Melanoma induces, and adenosine suppresses, CXCR3-cognate chemokine production and T-cell infiltration of lungs bearing metastatic-like disease. *Cancer Immunol Res.* 2015;3(8):956–967. doi:10.1158/2326-6066.CIR-15-0015.
14. Corey DM, Rinkevich Y, Weissman IL. Dynamic patterns of clonal evolution in tumor vasculature underlie alterations in lymphocyte-endothelial recognition to foster tumor immune escape. *Cancer Res.* 2016;76(6):1348–1353. doi:10.1158/0008-5472.CAN-15-1150.
15. González-Martín A, Gómez L, Lustgarten J, Mira E, Mañes S. Maximal T cell-mediated antitumor responses rely upon CCR5 expression in both CD4+ and CD8+ T cells. *Cancer Res.* 2011;71(16):5455–5466. doi:10.1158/0008-5472.CAN-11-1687.
16. Mikucki M, Fisher D, Matsuzaki J, Skitzki J, Gaulin N, Muhitch J, Ku A, Frelinger J, Odunsi K, Gajewski T. Non-redundant requirement for CXCR3 signalling during tumoricidal T-cell trafficking across tumour vascular checkpoints. *Nat Commun.* 2015;6:7458. doi:10.1038/ncomms8458.

17. Gazzaniga S, Bravo AI, Guglielmotti A, van Rooijen N, Maschi F, Vecchi A, Mantovani A, Mordoh J, Wainstok R. Targeting tumor-associated macrophages and inhibition of MCP-1 reduce angiogenesis and tumor growth in a human melanoma xenograft. *J Invest Dermatol.* 2007;127(8):2031–2041. doi:10.1038/sj.jid.5700827.
18. Nesbit M, Schaidler H, Miller TH, Herlyn M. Low-level monocyte chemoattractant protein-1 stimulation of monocytes leads to tumor formation in nontumorigenic melanoma cells. *J Immunol.* 2001;166(11):6483–6490. doi:10.4049/jimmunol.166.11.6483.
19. Dunleavey JM, Xiao L, Thompson J, Kim MM, Shields JM, Shelton SE, Irvin DM, Brings VE, Ollila DW, and Brekken RA. Vascular channels formed by subpopulations of PECAM1+ melanoma cells. *Nat Commun.* 2014;5:5200. doi:10.1038/ncomms6200.
20. Hillen F, Kaijzel EL, Castermans K, Oude Egbrink MG, Lowik CW, Griffioen AW. A transgenic Tie2-GFP athymic mouse model; a tool for vascular biology in xenograft tumors. *Biochem Biophys Res Commun.* 2008;368(2):364–367. doi:10.1016/j.bbrc.2008.01.080.
21. Ruf W, Seftor EA, Petrovan RJ, Weiss RM, Gruman LM, Margaryan NV, Seftor RE, Miyagi Y, Hendrix MJ. Differential role of tissue factor pathway inhibitors 1 and 2 in melanoma vasculogenic mimicry. *Cancer Res.* 2003;63(17):5381–5389.
22. Treps L, Faure S, Clere N. Vasculogenic mimicry, a complex and devious process favoring tumorigenesis - Interest in making it a therapeutic target. *Pharmacol Ther.* 2021;223:107805. doi:10.1016/j.pharmthera.2021.107805.
23. Wagenblast E, Soto M, Gutierrez-Angel S, Hartl CA, Gable AL, Maceli AR, Erard N, Williams AM, Kim SY, Dickopf S. A model of breast cancer heterogeneity reveals vascular mimicry as a driver of metastasis. *Nature.* 2015;520(7547):358–362. doi:10.1038/nature14403.
24. Francescone R, Scully S, Bentley B, Yan W, Taylor SL, Oh D, Moral L, Shao R. Glioblastoma-derived tumor cells induce vasculogenic mimicry through Flk-1 protein activation. *J Biol Chem.* 2012;287(29):24821–24831. doi:10.1074/jbc.M111.334540.
25. Misra RM, Bajaj MS, Kale VP. Vasculogenic mimicry of HT1080 tumour cells in vivo: critical role of HIF-1 $\alpha$ -neuropilin-1 axis. *PLOS ONE.* 2012;7(11):e50153. doi:10.1371/journal.pone.0050153.
26. Yang JP, Liao YD, Mai DM, Xie P, Qiang YY, Zheng LS, Wang MY, Mei Y, Meng DF, Xu L, et al. Tumor vasculogenic mimicry predicts poor prognosis in cancer patients: a meta-analysis. *Angiogenesis.* 2016;19(2):191–200. doi:10.1007/s10456-016-9500-2.
27. Warso MA, Maniotis AJ, Chen X, Majumdar D, Patel MK, Shilkaitis A, Gupta TKD, Folberg R. Prognostic significance of periodic acid-Schiff-positive patterns in primary cutaneous melanoma. *Clin Cancer Res.* 2001;7(3):473–477.
28. Denton KJ, Stretch JR, Gatter KC, Harris AL. A study of adhesion molecules as markers of progression in malignant melanoma. *J Pathol.* 1992;167(2):187–191. doi:10.1002/path.1711670205.
29. Harlin H, Meng Y, Peterson AC, Zha Y, Tretiakova M, Slingluff C, McKee M, Gajewski TF. Chemokine expression in melanoma metastases associated with CD8+ T-cell recruitment. *Cancer Res.* 2009;69(7):3077–3085. doi:10.1158/0008-5472.CAN-08-2281.
30. Langer HF, Orlova VV, Xie C, Kaul S, Schneider D, Lonsdorf AS, Fahrleitner M, Choi EY, Dutoit V, Pellegrini M, et al. A novel function of junctional adhesion molecule-C in mediating melanoma cell metastasis. *Cancer Res.* 2011;71(12):4096–4105. doi:10.1158/0008-5472.CAN-10-2794.
31. Hashizume H, Baluk P, Morikawa S, McLean JW, Thurston G, Roberge S, Jain RK, McDonald DM. Openings between defective endothelial cells explain tumor vessel leakiness. *Am J Pathol.* 2000;156(4):1363–1380. doi:10.1016/S0002-9440(10)65006-7.
32. Tan LY, Mintoff C, Johan MZ, Ebert BW, Fedele C, Zhang YF, Szeto P, Sheppard KE, McArthur GA, Foster-Smith E, et al. Desmoglein 2 promotes vasculogenic mimicry in melanoma and is associated with poor clinical outcome. *Oncotarget.* 2016;7(29):46492–46508. doi:10.18632/oncotarget.10216.
33. Ebert LM, Tan LY, Johan MZ, Min KK, Cockshell MP, Parham KA, Betterman KL, Szeto P, Boyle S, Silva L, et al. A non-canonical role for desmoglein-2 in endothelial cells: implications for neoangiogenesis. *Angiogenesis.* 2016;19(4):463–486. doi:10.1007/s10456-016-9520-y.
34. Litwin M, Clark K, Noack L, Furze J, Berndt M, Albelda S, Vadas M, Gamble J. Novel cytokine-independent induction of endothelial adhesion molecules regulated by platelet/endothelial cell adhesion molecule (CD31). *J Cell Biol.* 1997;139(1):219–228. doi:10.1083/jcb.139.1.219.
35. Martin-Ramirez J, Hofman M, van den Biggelaar M, Hebbel RP, Voorberg J. Establishment of outgrowth endothelial cells from peripheral blood. *Nat Protoc.* 2012;7(9):1709–1715. doi:10.1038/nprot.2012.093.
36. Martin M. Cutadapt removes adapter sequences from high-throughput sequencing reads. *EMBnet J.* 2011;17(1):10–12. doi:10.14806/ej.17.1.200.
37. Kim D, Pertea G, Trapnell C, Pimentel H, Kelley R, Salzberg SL. TopHat2: accurate alignment of transcriptomes in the presence of insertions, deletions and gene fusions. *Genome Biol.* 2013;14(4):1–13. doi:10.1186/gb-2013-14-4-r36.
38. Anders S, Pyl PT, Huber W. HTSeq—a Python framework to work with high-throughput sequencing data. *Bioinformatics.* 2015;31(2):166–169. doi:10.1093/bioinformatics/btu638.
39. Robinson MD, McCarthy DJ, Smyth GK. edgeR: a Bioconductor package for differential expression analysis of digital gene expression data. *Bioinformatics.* 2010;26(1):139–140. doi:10.1093/bioinformatics/btp616.
40. Chen Y, McCarthy D, Robinson M, Smyth GK. edgeR: differential expression analysis of digital gene expression data User's Guide. *Bioconductor User Guide* 2014:1–106.
41. Lun AT, Chen Y, Smyth GK. It's DE-licious: a recipe for differential expression analyses of RNA-seq experiments using quasi-likelihood methods in edgeR. *Methods Mol Biol.* 2016;1418:391–416. doi:10.1007/978-1-4939-3578-9\_19.
42. Thorvaldsdóttir H, Robinson JT, Mesirov JP. Integrative Genomics Viewer (IGV): high-performance genomics data visualization and exploration. *Brief Bioinform.* 2013;14(2):178–192. doi:10.1093/bib/bbs017.
43. Akbani R, Akdemir Kadir C, Aksoy BA, Albert M, Ally A, Amin Samirkumar B, Arachchi H, Arora A, Auman JT, Ayala B, et al. Genomic classification of cutaneous melanoma. *Cell.* 2015;161(7):1681–1696. doi:10.1016/j.cell.2015.05.044.
44. Iadocicco K, Monteiro LH, Chaui-Berlinck JG. A theoretical model for estimating the margination constant of leukocytes. *BMC Physiol.* 2002;2(3):3. doi:10.1186/1472-6793-2-3.
45. Hendrix MJ, Seftor RE, Seftor EA, Gruman LM, Lee LM, Nickoloff BJ, Miele L, Sheriff DD, Schatteman GC. Transendothelial function of human metastatic melanoma cells: role of the microenvironment in cell-fate determination. *Cancer Res.* 2002;62(3):665–668.
46. Sun B, Zhang D, Zhang S, Zhang W, Guo H, Zhao X. Hypoxia influences vasculogenic mimicry channel formation and tumor invasion-related protein expression in melanoma. *Cancer Lett.* 2007;249(2):188–197. doi:10.1016/j.canlet.2006.08.016.
47. Vartanian A, Stepanova E, Grigorieva I, Solomko E, Baryshnikov A, Lichinitser M. VEGFR1 and PKC $\alpha$  signaling control melanoma vasculogenic mimicry in a VEGFR2 kinase-independent manner. *Melanoma Res.* 2011;21(2):91–98. doi:10.1097/CMR.0b013e328343a237.
48. Zheng F, Jang W-C, Fung FK, Lo AC, Wong IY. Up-regulation of ENO1 by HIF-1 $\alpha$  in retinal pigment epithelial cells after hypoxic challenge is not involved in the regulation of VEGF secretion. *PLoS One.* 2016;11(2):e0147961. doi:10.1371/journal.pone.0147961.



49. C-j H, Wang L-Y, Chodosh LA, Keith B, Simon MC. Differential roles of hypoxia-inducible factor 1 $\alpha$  (HIF-1 $\alpha$ ) and HIF-2 $\alpha$  in hypoxic gene regulation. *Mol Cell Biol.* 2003;23(24):9361–9374. doi:10.1128/MCB.23.24.9361-9374.2003.
50. Bianchi E, Molteni R, Pardi R, Dubini G. Microfluidics for in vitro biomimetic shear stress-dependent leukocyte adhesion assays. *J Biomech.* 2013;46(2):276–283. doi:10.1016/j.jbiomech.2012.10.024.
51. Jain RK. Determinants of tumor blood flow: a review. *Cancer Res.* 1988;48:2641–2658.
52. Kleiveland CR. Peripheral Blood Mononuclear Cells. In: Verhoecx K, Cotter P, López-Expósito I, Kleiveland C, Lea T, Mackie A, Requena T, Swiatecka D, Wichers H, editors. The impact of food bioactives on health: in vitro and ex vivo models. Cham, Switzerland: Springer International Publishing; 2015. 161–167.
53. Kroon J, Schaefer A, van Rijssel J, Hoogenboezem M, van Alphen F, Hordijk P, Stroes ESG, Strömblad S, van Rheenen J, van Buul JD. Inflammation-sensitive Myosin-X functionally supports leukocyte extravasation by Cdc42-mediated ICAM-1-rich endothelial filopodia formation. *J Immunol.* 2018;200(5):2031–2041. doi:10.4049/jimmunol.1700702.
54. Kuhn A, Brachtendorf G, Kurth F, Sonntag M, Samulowitz U, Metze D, Vestweber D. Expression of endomucin, a novel endothelial sialomucin, in normal and diseased human skin. *J Invest Dermatol.* 2002;119(6):1388–1393. doi:10.1046/j.1523-1747.2002.19647.x.
55. Garraway LA, Widlund HR, Rubin MA, Getz G, Berger AJ, Ramaswamy S, Beroukhi R, Milner DA, Granter SR, Du J, et al. Integrative genomic analyses identify MITF as a lineage survival oncogene amplified in malignant melanoma. *Nature.* 2005;436(7047):117–122. doi:10.1038/nature03664.
56. Maniotis AJ, Folberg R, Hess A, Seftor EA, Gardner LM, Pe'er J, Trent JM, Meltzer PS, Hendrix MJ. Vascular channel formation by human melanoma cells in vivo and in vitro: vasculogenic mimicry. *Am J Pathol.* 1999;155(3):739–752. doi:10.1016/S0002-9440(10)65173-5.
57. Lin Y, Xu J, Lan H. Tumor-associated macrophages in tumor metastasis: biological roles and clinical therapeutic applications. *J Hematol Oncol.* 2019;12(1):76. doi:10.1186/s13045-019-0760-3.
58. Conroy MJ, Lysaght J. CX3CL1 signaling in the tumor microenvironment. *Adv Exp Med Biol.* 2020;1231:1–12. doi:10.1007/978-3-030-36667-4\_1.
59. Kim MJ, Sun HJ, Song YS, Yoo S-K, Kim YA, Seo J-S, Park YJ, Cho SW. CXCL16 positively correlated with M2-macrophage infiltration, enhanced angiogenesis, and poor prognosis in thyroid cancer. *Sci Rep.* 2019;9(1):1–10. doi:10.1038/s41598-018-37186-2.
60. Huang Y, Zhu X-Y, Du M-R, Li D-J. Human trophoblasts recruited T lymphocytes and monocytes into decidua by secretion of chemokine CXCL16 and interaction with CXCR6 in the first-trimester pregnancy. *J Immunol.* 2008;180(4):2367–2375. doi:10.4049/jimmunol.180.4.2367.
61. Panek CA, Ramos MV, Mejias MP, Abrey-Recalde MJ, Fernandez-Brando RJ, Gori MS, Salamone GV, Palermo MS. Differential expression of the fractalkine chemokine receptor (CX 3 CR1) in human monocytes during differentiation. *Cell Mol Immunol.* 2015;12(6):669–680. doi:10.1038/cmi.2014.116.
62. Yang XL, Liu KY, Lin FJ, Shi HM, Ou ZL. CCL28 promotes breast cancer growth and metastasis through MAPK-mediated cellular anti-apoptosis and pro-metastasis. *Oncol Rep.* 2017;38(3):1393–1401. doi:10.3892/or.2017.5798.
63. Ren L, Yu Y, Wang L, Zhu Z, Lu R, Yao Z. Hypoxia-induced CCL28 promotes recruitment of regulatory T cells and tumor growth in liver cancer. *Oncotarget.* 2016;7(46):75763–75773. doi:10.18632/oncotarget.12409.
64. Huang G, Tao L, Shen S, Chen L. Hypoxia induced CCL28 promotes angiogenesis in lung adenocarcinoma by targeting CCR3 on endothelial cells. *Sci Rep.* 2016;6(1):27152. doi:10.1038/srep27152.
65. Ganss R, Ryschich E, Klar E, Arnold B, Hämmerling GJ. Combination of T-cell therapy and trigger of inflammation induces remodeling of the vasculature and tumor eradication. *Cancer Res.* 2002;62:1462–1470.
66. Hong M, Puaux A-L, Huang C, Loumagne L, Tow C, Mackay C, Kato M, Prévost-Blondel A, Avril M-F, Nardin A, et al. Chemotherapy induces intratumoral expression of chemokines in cutaneous melanoma, favoring T-cell infiltration and tumor control. *Cancer Res.* 2011;71(22):6997–7009. doi:10.1158/0008-5472.CAN-11-1466.
67. Huang H, Langenkamp E, Georganaki M, Loskog A, Fuchs PF, Dieterich LC, Kreuger J, Dimberg A. VEGF suppresses T-lymphocyte infiltration in the tumor microenvironment through inhibition of NF- $\kappa$ B-induced endothelial activation. *FASEB J.* 2015;29(1):227–238. doi:10.1096/fj.14-250985.
68. Liu C, Peng W, Xu C, Lou Y, Zhang M, Wargo JA, Chen JQ, Li HS, Watowich SS, Yang Y, et al. BRAF inhibition increases tumor infiltration by T cells and enhances the antitumor activity of adoptive immunotherapy in mice. *Clin Cancer Res.* 2013;19(2):393–403. doi:10.1158/1078-0432.CCR-12-1626.
69. Wu X, Giobbie-Hurder A, Liao X, Lawrence DP, McDermott DF, Zhou J, Rodig SJ, Hodi FS. VEGF neutralization plus CTLA-4 blockade alters soluble and cellular factors associated with enhancing lymphocyte infiltration and humoral recognition in melanoma. *Cancer Immunol Res.* 2016;4(10):858–868. doi:10.1158/2326-6066.CIR-16-0084.
70. Graziani G, Ruffini F, Tentori L, Scimeca M, Dorio AS, Atzori MG, Failla CM, Morea V, Bonanno E, D'Atri S, et al. Antitumor activity of a novel anti-vascular endothelial growth factor receptor-1 monoclonal antibody that does not interfere with ligand binding. *Oncotarget.* 2016;7(45):72868–72885. doi:10.18632/oncotarget.12108.
71. Lacial PM, Atzori MG, Ruffini F, Scimeca M, Bonanno E, Cicconi R, Mattei M, Bernardini R, D'Atri S, Tentori L, et al. Targeting the vascular endothelial growth factor receptor-1 by the monoclonal antibody D16F7 to increase the activity of immune checkpoint inhibitors against cutaneous melanoma. *Pharmacol Res.* 2020;159:104957. doi:10.1016/j.phrs.2020.104957.
72. Straetemans T, Berrevoets C, Coccoris M, Treffers-Westerlaken E, Wijers R, Cole DK, Dardalhon V, Sewell AK, Taylor N, Verweij J, et al. Recurrence of melanoma following T cell treatment: continued antigen expression in a tumor that evades T cell recruitment. *Mol Ther.* 2015;23(2):396–406. doi:10.1038/mt.2014.215.